

# Inertia gravity wave generation by the tropospheric midlatitude jet as given by the Fronts and Atlantic Storm-Track Experiment radio soundings

R. Plougonven

Advanced Study Program, Mesoscale and Microscale Meteorology Division, National Center for Atmospheric Research, Boulder, Colorado, USA

H. Teitelbaum and V. Zeitlin

Laboratoire de Météorologie Dynamique, Ecole Normale Supérieure, Paris, France

Received 25 February 2003; revised 14 August 2003; accepted 20 August 2003; published 15 November 2003.

[1] Generation of inertia gravity waves by the midlatitude tropospheric jet is studied on the basis of the data obtained from the radio soundings over the North Atlantic during the Fronts and Atlantic Storm-Track Experiment campaign. A sample of 224 radio soundings is used to analyze the wave activity as a function of the distance to the jet. It is shown that radio soundings displaying the most intense gravity wave activity, both in the stratosphere and in the troposphere, are the ones closest to the jet axis. Thus the jet region is the dominant source of gravity waves in this region far from orography. Further examination allows for identification of two specific regions of the flow that are associated with intense gravity wave activity: the vicinity of the maximum of the jet velocity and the regions of strong curvature of the jet. The detailed case studies we provide suggest that geostrophic adjustment is the dynamical mechanism responsible for the generation of large-amplitude inertia gravity waves in the regions of the strong curvature of the wind. The generation of waves in the vicinity of the regions where the wind veers, in the deep troughs of the geopotential, appears to be systematic. *INDEX TERMS:* 3329 Meteorology and Atmospheric Dynamics: Mesoscale meteorology; 3334 Meteorology and Atmospheric Dynamics: Middle atmosphere dynamics (0341, 0342); 3384 Meteorology and Atmospheric Dynamics: Waves and tides;

*KEYWORDS:* geostrophic adjustment, inertia gravity waves, jet stream

**Citation:** Plougonven, R., H. Teitelbaum, and V. Zeitlin, Inertia gravity wave generation by the tropospheric midlatitude jet as given by the Fronts and Atlantic Storm-Track Experiment radio soundings, *J. Geophys. Res.*, 108(D21), 4686, doi:10.1029/2003JD003535, 2003.

## 1. Introduction

[2] Gravity waves are ubiquitous and play an essential role in the dynamics of the middle atmosphere. In particular, one cannot explain the atmosphere's global circulation without taking into account the momentum transport and deposit due to waves [cf., e.g., *Andrews et al.*, 1987]. Transport and mixing due to gravity waves, and especially to inertia gravity waves (we use the standard jargon and call the high-frequency inertia gravity waves simply gravity waves and those with frequencies close to the Coriolis frequency  $f$ , inertia gravity waves; the abbreviation IGW will be frequently used below for both) (IGW), although difficult to quantify at present, are expected to be important, particularly in the lower stratosphere [*Danielsen et al.*, 1991; *Pierce and Fairlie*, 1993]. Another important effect of IGW in the lower stratosphere is their contribution via breaking to the formation of the clear air turbulence.

Although the sources of IGW are qualitatively understood, their quantification remains an open problem, especially in what concerns the nonorographic ones.

[3] Observations provide evidence that jets and fronts are quantitatively important sources of IGW: *Fritts and Nastrom* [1992] used aircraft measurements to assess the contributions of four sources of mesoscale gravity waves: jet streams, fronts, convection and orography. They showed that the mesoscale variance of the horizontal velocity and temperature was enhanced almost by an order of magnitude in the vicinity of fronts and jets. Similarly, *Eckerman and Vincent* [1993] used radar measurements over southern Australia to show that energetic gravity wave motions throughout the troposphere occurred during the passage of the cold fronts. Yet, the statistical analysis of the MU radar data over a 3-year period by *Sato* [1994] showed that the correlation between the intensity of the jet and that of the waves is significant, in that data, on the seasonal scale only.

[4] Spatial variability of the IGW field produced by the jet stream is not sufficiently known, in particular in what

concerns its persistent characteristic features, if any. Configurations of the jet leading to intense IGW activity are not clearly identified, although the exit region of the jet stream has been put forward in this context in several studies, numerical [O'Sullivan and Dunkerton, 1995; Zhang et al., 2001] as well as observational [Uccellini and Koch, 1987; Thomas et al., 1999; Guest et al., 2000; Pavelin et al., 2001; Hertzog et al., 2001].

[5] Even if a given region of the flow is known to generate IGW, the problem of identifying the precise dynamical mechanism of the wave emission remains. Several dynamical mechanisms related to the front jet activity may be at the origin of the observed waves: shear instability [Lalas and Einaudi, 1976; Fritts, 1982; Sutherland and Peltier, 1995; Lott, 1997; Bühler et al., 1999; Scinocca and Ford, 2000], symmetric instability [Ciesielski et al., 1989], convection [Fovell et al., 1992; Pfister et al., 1993; Lane et al., 2001] and geostrophic adjustment [Van Tuyl and Young, 1982; Uccellini and Koch, 1987; Fritts and Luo, 1992; O'Sullivan and Dunkerton, 1995]. Furthermore, these mechanisms may act simultaneously, giving no possibility to clearly isolate one of them. For example, the Kelvin-Helmholtz instability excites waves by nonlinear interactions of unstable modes of different horizontal wavelengths, as shown by the two-dimensional numerical simulations of Scinocca and Ford [2000], but is also expected to lead to the excitation of the gravity waves via the geostrophic adjustment of the arising turbulent zones [Bühler et al., 1999].

[6] A number of studies, both observational [Uccellini and Koch, 1987; Thomas et al., 1999; Pavelin et al., 2001; Hertzog et al., 2001] and numerical [Van Tuyl and Young, 1982; Fritts and Luo, 1992; Luo and Fritts, 1993; O'Sullivan and Dunkerton, 1995], put forward the geostrophic adjustment process as a major source of inertia gravity waves in the jet region. Geostrophic adjustment is the process of relaxation of unbalanced initial conditions toward some balanced state [e.g., Rossby, 1938; Blumen, 1972; Fritts and Luo, 1992; Reznick et al., 2001]. The IGW (by definition, unbalanced) propagate away from the initial perturbation, and the relaxation is expected to take place on a timescale of the order of the inertial period. Geostrophic adjustment can occur when the large-scale flow departs from balance and/or generates some regions of imbalance, which happens, for example, during frontogenesis or jet streaks evolution. Another source of imbalance, produced by mountain wave activity and subsequent adjustment was considered in [Scavuzzo et al., 1998].

[7] The classical scenario of the deformation frontogenesis obtained in the framework of the semigeostrophic approximation by filtering IGW altogether [Hoskins and Bretherton, 1972] corresponds, in fact, to the passage from a regular to a singular adjusted state due to the action of the external deformation field. (The singular state (front) may result from the geostrophic adjustment without deformation, as well (spontaneous frontogenesis) [cf. Blumen and Wu, 1995; Kalashnik, 1998, 2000; LeSommer et al., 2003].) The necessity to understand the IGW emission by frontogenesis, i.e., to understand the difference between the full (primitive equations) and semigeostrophic descriptions of the frontogenesis has motivated theoretical [e.g., Ley and Peltier, 1978] and numerical [Gall et al., 1988; Garner, 1989;

Snyder et al., 1993; Griffiths and Reeder, 1996; Reeder and Griffiths, 1996] work on two-dimensional models of the atmosphere in the same setting (flat bottom, rigid lid) as in the classical paper of Hoskins and Bretherton [1972]. Griffiths and Reeder [1996] and Reeder and Griffiths [1996] improved the preceding studies by simulating both the surface and upper-level frontogenesis, and by including propagation of waves excited by the jet/front system into the stratosphere. As discussed by Snyder et al. [1993] and explicitly shown by the comparison of various scenarios of frontogenesis by Reeder and Griffiths [1996], the IGW emission intensifies when the timescale of the evolution of the background flow becomes comparable to or faster than the inertial period.

[8] A number of papers studied the IGW generation triggered by the instabilities of the jet. Van Tuyl and Young [1982] used the two-layer primitive equation model to simulate the propagation of a jet streak and the emission of waves in the jet via geostrophic adjustment. The propagation of the jet streaks induces ageostrophic motions; if sufficiently slow, they are described with the help of the balanced dynamics (e.g., the quasi-geostrophic dynamics) as forced secondary circulations. However, in the regions such as jet streaks, the Lagrangian accelerations can become so strong that the ageostrophic circulation predicted by the balanced models is unable to maintain the balance condition, and inertia gravity waves are excited. Using a full GCM, O'Sullivan and Dunkerton [1995] studied the generation of inertia gravity waves from a jet during the development of an unstable baroclinic wave. IGW appeared at the mature stage of the unstable baroclinic wave when the upper-tropospheric jet became severely distorted (a deep trough has formed in the upper-tropospheric geopotential field). These simulations suggested that the geostrophic adjustment is an essential mechanism of the IGW generation for the lower stratosphere (almost no IGW emission toward the troposphere was observed), and that the exit region of the upper-tropospheric jet was the main region of the flow where this mechanism manifested itself. Furthermore, O'Sullivan and Dunkerton [1995] argued that thus produced IGW, because of the large particle displacements they engender and, eventually, because of the breaking or the shear instability they induce, can play an important role in mixing in the lower stratosphere. Using a mesoscale model, Zhang et al. [2001] studied in great detail a specific event of the tropospheric gravity wave generation, amplification and maintenance. In this particular case, the jet exit region again was the key one for the generation of the waves by the geostrophic adjustment.

[9] In what concerns the diagnostics of the unbalanced flow zones, the Lagrangian Rossby number (the ratio of the Lagrangian acceleration to the Coriolis force) was shown to be an efficient tool in the studies by O'Sullivan and Dunkerton [1995] and by Reeder and Griffiths [1996]. However, Koch and Dorian [1988] pointed out that this criterion overrepresented the regions of strong flow curvature, where  $\mathbf{v}$  is expected to follow the gradient wind balance rather than the simple geostrophic balance. As the error was due to the along-stream wind it was proposed to detect the flow imbalance using a cross-stream Lagrangian Rossby number  $Ro_{\perp}$  calculated from the component of the ageostrophic wind perpendicular to the total wind. A recent

numerical study [Zhang *et al.*, 2000] focusing explicitly on the efficiency of various imbalance diagnostics has confirmed that the cross-stream Lagrangian Rossby number is a reliable diagnostic of flow imbalance. This diagnostics can be also used to determine the regions favorable to the IGW generation by the geostrophic adjustment process from the coarse-resolution descriptions of the large-scale flow as given, e.g., by the analyses of the European Center for Medium-Range Weather Forecast (ECMWF).

[10] Several recent papers have investigated in detail observations of individual cases of wave generation by regions where the jet is severely distorted, and referred to *O'Sullivan and Dunkerton* [1995] in order to identify the geostrophic adjustment as the IGW generation mechanism. *Thomas et al.* [1999] have analyzed emission of the IGW from the tropospheric jet stream using radar measurements. The waves emanated from the jet exit region, where the jet veers toward a trough of the geopotential, very similar to the region put forward by *O'Sullivan and Dunkerton* [1995]. The authors stressed two points that contrast with the previous observations of IGW: first, the waves were observed propagating not only upward in the lower stratosphere, but also downward in the troposphere, with similar amplitudes (about  $2 \text{ ms}^{-1}$ ). This observation is consistent with the theoretical studies [*Fritts and Luo*, 1992] of the geostrophic adjustment, but differs from the simulations of *O'Sullivan and Dunkerton* [1995]. Second, the wave vector was parallel to the jet, rather than being perpendicular, as often supposed to be the case for waves generated by the geostrophic adjustment [*Fritts and Luo*, 1992; *Sato*, 1994]. *Pavelin et al.* [2001] presented the radar observations of a large amplitude (up to  $10 \text{ ms}^{-1}$ ) wave persisting for several days in the lower stratosphere and generated in a region where the jet was highly distorted. Both of these studies rely on the similarity of the large-scale flow configuration to that seen in *O'Sullivan and Dunkerton's* [1995] simulations while identifying the geostrophic adjustment as the generation mechanism. *Hertzog et al.* [2001] made an attempt to determine more precisely the origin of an inertia gravity wave that had been observed at altitudes 18–20 km in the lidar in situ measurements. Using the background fields provided by the ECMWF analyses, they conducted a ray-tracing reconstruction which indicated that the tentative source was located at the exit region of a jet streak directed southeastward, in a deep trough of the geopotential. A diagnostics of the flow imbalance was used to support the conclusions of the WKB analysis.

[11] Another aspect of the geostrophic adjustment which was revealed recently in the opposite situation of the intense rectilinear jets when studying them in the framework of simplified models [cf. *Zeitlin et al.*, 2003; *LeSommer et al.*, 2003], is the specific role of the anticyclonic side of the jet which favors wave breaking even in the absence of symmetric instability.

[12] The database of the Fronts and Atlantic Storm-Track Experiment (FASTEX) [*Joly et al.*, 1997, 1999], which was carried out between 5 January and 27 February 1997 provides a unique tool for studying nonorographic IGW [e.g., *Moldovan et al.*, 2002] as a large number of high-resolution radio soundings were made from the ships cruising in the North Atlantic (i.e., far from orographic

wave sources). It may be used to check the above-described theoretical and numerical predictions as well as consolidate the previous observational evidence of the IGW activity.

[13] In the present work we use the FASTEX data to investigate the spatial variability of the IGW activity in the tropospheric jet region. Our goals are to study the jet as a wave source, to analyze the role of the geostrophic adjustment in the IGW generation and to assess the typical parameters of the IGW emitted by the jet.

[14] Our strategy was to study the intensity of waves detected by the FASTEX soundings as a function of the synoptic situation in the upper troposphere. This synoptic situation was recovered from the ECMWF analyses. We first describe the data and the processing procedure (section 2). Then a general analysis of the wave intensity retrieved from the data as a function of the distance to the jet is given (section 3). This analysis allows to identify two regions of the flow associated with high wave activity: those close to the maxima of the velocity and those of high distortion of the jet. A detailed case study of the IGW observed in the high-distortion region is carried out in section 4, and suggests that geostrophic adjustment is the source. A comparison with other similar cases in the data set is presented in section 5, suggesting that generation of waves by geostrophic adjustment in this region is recurrent. Section 6 contains summary and discussion.

## 2. Description of the Data Set and the Processing Procedure

### 2.1. Radio Soundings

[15] In order to eliminate the orographic IGW sources, only the radio soundings launched from ships, between  $30^\circ\text{N}$  and  $70^\circ\text{N}$  in latitude and  $50^\circ\text{W}$  and  $0^\circ$  in longitude were selected. Among the radio soundings available for the period from 1 to 25 February 1997 in that region, we retained only those containing uninterrupted acquisition of the horizontal wind up to the altitude of 20 km. This choice was a compromise allowing us to have, at the same time, sufficient amount of data for the stratospheric heights and a large enough number of soundings. The geographical positions of the launching locations of the radio soundings used in the subsequent analysis are shown in Figure 1.

[16] In order to separate the background flow and the wave perturbation, the radio soundings were processed in the following way: the observed profiles were first interpolated, using a cubic spline in order to have equally spaced points with a resolution of 50 m, which was the typical resolution of the original profiles. A high-pass filter was then used to suppress perturbations with scales larger than 5 km. This upper bound was chosen because the preliminary analysis of the individual soundings showed that the typical wavelengths of the identified waves were 1–4 km or shorter [see also *Sato*, 1994]. Moreover, using a larger value would allow regions of strong vertical shear associated with the jet to make a contribution to the disturbance velocity; this is to be avoided as we will identify the disturbance velocity with gravity waves. The filter we apply is nonrecursive, in order to preserve the phase of the harmonics of the signal, and uses the Kaiser

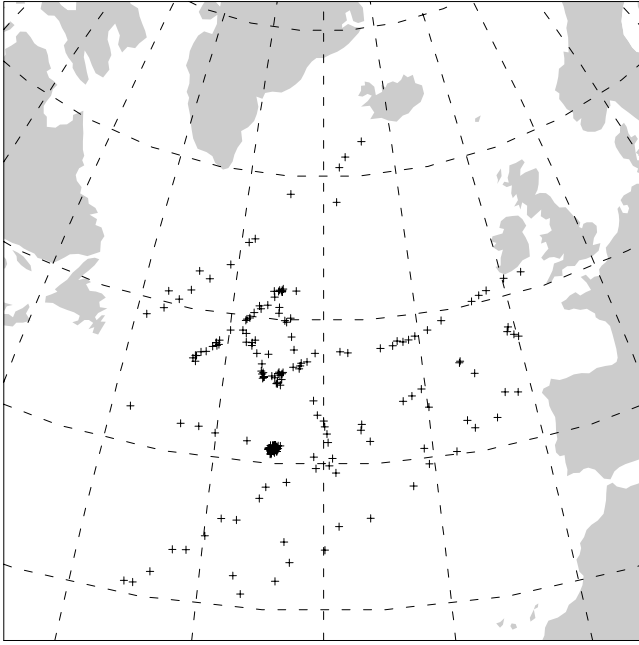


**Figure 1.** Locations of the 224 radio soundings used in the subsequent analysis, all launched from ships, between 1 and 25 February. Lines of longitude and latitude are indicated every 10°.

window [Hamming, 1983]. The parameters are adjusted in a way to avoid the Gibbs effect. The details as regards to the filter and its transfer function may be found in [Scavuzzo *et al.*, 1998].

[17] Two segments were isolated in each radio sounding: a tropospheric segment extending from 1 to 9 km and a stratospheric segment from 12 to 20 km. The upper and lower bounds were chosen so that they normally exclude the tropopause from both segments, and the surface boundary layer from the tropospheric segment.

[18] The wave activity  $A$  in each segment was defined using the variance of the perturbation velocity  $\mathbf{v}'$ :

$$A = \frac{1}{z_2 - z_1} \int_{z_1}^{z_2} |\mathbf{v}'|^2 dz. \quad (1)$$

The motivation for defining  $A$  is to have an easily calculable quantity measuring the intensity of waves in the flow, which would allow for a comparison of different regions of the flow. The small-scale turbulence, or intense shearing associated with the jet are potential sources of systematic errors in such procedure. However, the individual inspection of the observed profiles shows that the contribution of the IGW largely dominates. In particular, as noted above, the threshold chosen for the filter mostly excludes the contribution of the shear associated with the jet. We finally note that other methods of filtering and other thresholds have also been tested, which leave the results qualitatively unchanged.

## 2.2. Jet Diagnostics and Classification of the Radio Soundings in Terms of the Distance From the Jet Axis

[19] In contrast with a number of preceding studies our goal is to analyze the IGW field dependence on the synoptic

situation in the upper troposphere, and not on the season or absolute position.

[20] Surface fronts and the upper-level jets are dynamically connected. They are expected to be the major sources of the IGW activity over the ocean. In the numerical simulations of inertia gravity wave generation by an unstable baroclinic wave *O'Sullivan and Dunkerton* [1995] showed explicitly that the waves that appeared in the lower stratosphere were generated by the jet, and not by the surface front: they repeated their simulation with an artificial damping of the divergence field in the 5 km close to the surface, thus eliminating any gravity wave radiation from the surface fronts, and found that the waves which appeared in the lower stratosphere were almost unchanged. Further indication that lower-stratospheric waves are primarily generated at the level of the jet is given by the simulations and the ray-tracing calculations of *Reeder and Griffiths* [1996, cf. Figure 1]. These simulations had finer resolution, and the frontogenesis was better resolved than by [O'Sullivan and Dunkerton, 1995]. It nevertheless appeared from their ray-tracing calculations that the lower-stratospheric waves were produced at the jet location, rather than by the surface fronts. By these reasons, we have chosen to examine the intensity of the waves as a function of the distance of the radio soundings to the jet axis.

[21] The jet axis was defined as the crest line of the isolines of the norm of the velocity on the isobaric surface corresponding to  $Z = 9$  km in the log pressure coordinates ( $\sim 250$  hPa). This choice is discussed below.

[22] Other fields could be used to identify the jet: the geopotential height on the isobaric surfaces, the potential vorticity (PV) or the relative vorticity on the isentropic surfaces, (for example, one may take the 310 K surface (see Figure 7)). We have checked that the agreement between these descriptions and our definition of the jet is satisfactory, in particular in the regions of intense jet (e.g., compare Figures 6 and 7).

[23] The  $Z = 9$  km surface was chosen after examining a number of samples: the wind intensity was often maximal between 8 and 9 km, and vertical variation of the location of the jet was generally small at this altitude. Nevertheless, significant vertical variations in the intensity of the jet were sometimes observed.

[24] Obviously, there are periods and locations where it is difficult to define the jet properly. However, the radio soundings in such locations were rather rare and generally exhibited a low wave activity. Hence we estimate the influence of such soundings on the results below as minor.

[25] The distance of each radio sounding to the jet was calculated as the distance between the position of the radiosonde (averaged over the first 20 km of its ascent) and the position of the point closest to that on the jet axis. The radiosondes were advected horizontally as they were mounting, particularly those launched close to the core of the jet. The advection can be considerable in absolute value (for our sample of soundings, its maximum value was 280 km, and the mean was 130 km). However, this motion is essentially parallel to the jet axis, and leaves the distance to the jet nearly unchanged. We checked this by calculating the distance to the jet for several soundings by using first the coordinates of the launching position, and then those of

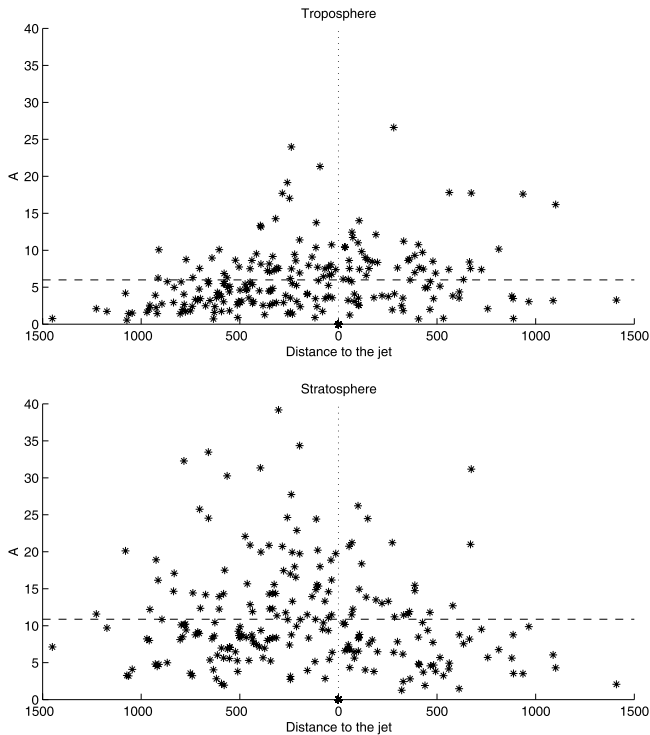


**Figure 2.** Distribution of the gravity wave activity  $A$ , in  $\text{m}^2 \text{s}^{-2}$ , as a function of distance to the jet, in km, for the (top) troposphere and the (bottom) stratosphere. The average values of  $A$ ,  $6.0 \text{ m}^2 \text{ s}^{-2}$  and  $10.9 \text{ m}^2 \text{ s}^{-2}$ , respectively, are indicated by dashed lines.

the last measurement. The difference between the results was always less than 15 km (less than 10%). Another possible source of uncertainty is the time resolution of the ECMWF analyses.

### 3. Analysis of the Bulk of the Data

#### 3.1. Intensity of the Gravity Wave Field as a Function of the Distance to the Jet Axis

[26] By using the methodology presented in the previous section, we obtained the intensity of the wave activity as a function of the distance to the tropospheric jet above the North Atlantic. It is plotted in Figure 2 for all of the 224 radio soundings that we analyzed.

[27] The distributions have the following characteristic features: (1) Wave activity is enhanced in the vicinity of the jet axis. (2) Wave activity is more pronounced in the stratosphere than in the troposphere. This observation is consistent with the increase of the amplitude of upward-propagating waves because of decreasing density, and with stronger stratification. (3) In the troposphere, the highest values of  $A$  are close to the jet axis, but  $A$  is on average higher on the cyclonic side. It is uncertain, however, whether this asymmetry is representative: Indeed, our set of radio soundings has more points on the anticyclonic side than on the cyclonic side (143 against 81), and the higher values of  $A$  on the cyclonic side are due essentially to five soundings with very high values of  $A$ . (4) In the stratosphere, the distribution of  $A$  is shifted toward the anticyclonic side of the jet (negative distances). The maximum is

located approximately at  $-300$  km. The anticyclonic side of the jet is well sampled and we believe this tendency to be representative.

[28] In order to make the main characteristic features of these distributions come out more clearly, the whole set of radio soundings has then been divided into eight bins of 28 each; for every bin, the mean value of  $A$  and its standard deviation were calculated (compare Figure 3). The peak of the stratospheric distribution in the anticyclonic side appears clearly.

[29] We have tested the sensitivity of the distributions shown in Figures 2 and 3 to the choice of the filter and/or its parameters. Using the same filter, the soundings were processed taking 7.5 km as the upper bound. As a test of other filters, we have also subtracted the background flow using polynomial fits of various orders (fit of order 3 and 4 on each segment of 8 km, and a polynomial fit of order 5 on the whole profile (20 km)), as was done by [Guest *et al.*, 2000] for instance. The essential qualitative features outlined above, and particularly the shift of the distribution in the stratosphere to the anticyclonic side, were systematically observed. On the other hand, the distributions varied quantitatively: variances  $A$  were greater for the order 5 polynomial fit and for the filter with 7.5 km as the upper bound, and lower for the polynomial fits of order 3 and 4.

[30] The sensitivity of these distributions to the choice of the tropospheric and stratospheric segments was also tested:

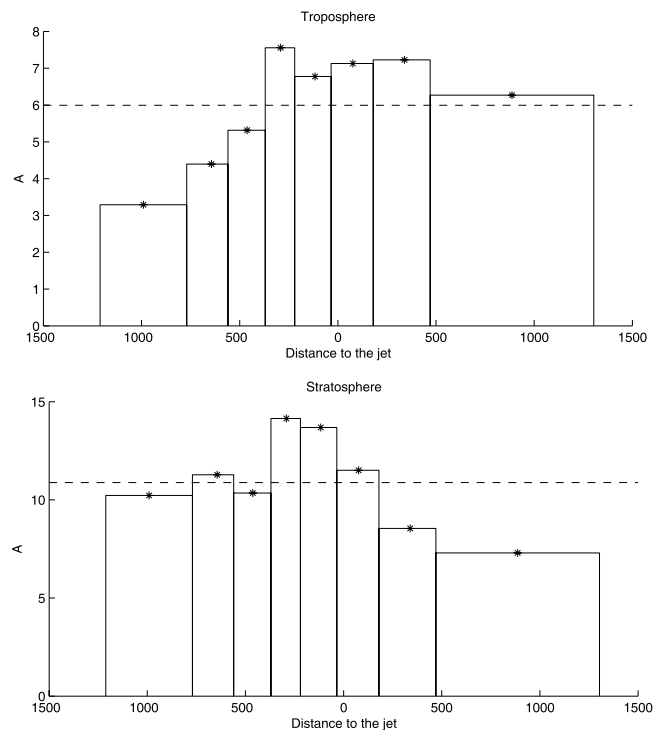


**Figure 3.** Histograms of  $A$  averaged in eight bins containing 28 radio soundings each for the (left) troposphere and the (right) stratosphere. The average value of  $A$  for each case is given by the dashed line. The stars indicate the mean distance to the jet for the soundings of a given box. Note that the vertical scale is not the same in the two plots.

instead of using 8-km-long segments (from 1 to 9 km and from 12 to 20 km), segments of 2 km (four in the troposphere, from 1 to 3 km, 3 to 5 km, etc., and four in the stratosphere) were used for the same analysis. The corresponding plots of the IGW activity as a function of distance to the jet preserved the main qualitative features discussed above. Moreover, they gave indications on the variation of IGW activity with height. In the troposphere, the values of  $A$  increased with height. In the stratosphere, the highest values for the variance were observed in the lower stratosphere (12–16 km), with the strongest shift to the anticyclonic side. Both of these observations are consistent with the jet being the source of the waves. Furthermore, the fact that the highest values were observed in the lower stratosphere can be explained by occurrence of critical levels and wave breaking higher on [cf., e.g., Moldovan *et al.*, 2002].

[31] Various mechanisms can be put forward in order to explain the observed features of the wave activity distribution. First, the cold fronts, which are known to be sources of waves, precede the jet on its anticyclonic side, and the shift in the distribution could hence be due to the IGW generation by the surface fronts. However, one would then expect to see a similar shift in the troposphere, which is not the case.

[32] Second, the anticyclonic region has an effective Coriolis parameter ( $f + \partial_x v - \partial_y u$ ) that is lower than  $f$ . It was shown by Kunze [1985], by using the WKB approach for near-inertial waves in a uniform geostrophic shear that the latter can trap and amplify waves. In real atmospheric situations, although jets are neither rectilinear nor stationary, the anticyclonic side of the jet is also expected to be the location of enhanced wave activity (‘leaky’ waveguide [Dunkerton, 1984]). This is consistent with the distribution of the wave activity we obtain.

[33] It should be emphasized that the stratospheric slice of data is “cleaner” for identification of the wave activity related to the proper dynamics of the jet. The difficulty of separating waves and the background flow (see section 2.1) and various secondary effects can interfere in the troposphere: (multiple) reflection of the waves emitted by the jet from the surface, their interactions with the boundary layer etc. Therefore in what follows we pay much more attention to the stratospheric data.

### 3.2. Identification of the Regions of the Flow Favorable to Wave Generation

[34] Further information may be obtained from the above analysis by identifying the particular configurations of the flow corresponding to the radio soundings with highest values of  $A$  [cf. Guest *et al.*, 2000]. Plotting the variation of the wave activity against time showed that soundings with high wave activity were grouped in time in about six episodes, each lasting about 2 days. Using the corresponding analyses of the ECMWF we identified two specific regions of the flow that are favorable to high wave activity.

[35] 1. The vicinity of the maxima of the jet velocity: the highest values of  $A$  were found for soundings close to the maxima of the wind. The curvature of the jet in those regions is generally weak. We retained in this category the radio soundings located in the vicinity of the regions where

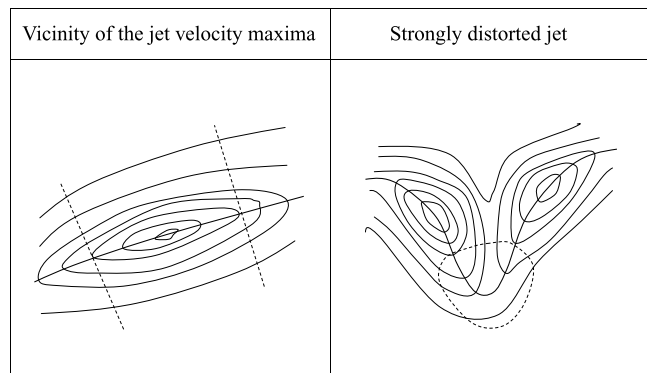


**Figure 4.** Schematic representation of the two regions of the flow identified as most favorable to high gravity wave activity, as seen in maps of the norm of the wind on an isobaric surface (thin lines are isolines of the norm of the wind; the thicker line defines the jet). The regions of interest are indicated by dashed lines.

the jet velocity was 80% of the maximum or higher (see Figure 4; 91 radio soundings in total). It should be noted that the choice of the fixed  $Z = 9$  km surface may somewhat influence the results as the location of the wind maximum along the jet can vary with height.

[36] 2. The regions of high curvature of the jet: those can be seen on the maps of geopotential as deep troughs propagating over the Atlantic in about 2 days or, equivalently, on the isentropic maps of PV (i.e., about the 320 K surface) as equatorward excursions of the high-PV air. Such configurations of the jet appeared recurrently (51 radio soundings in total); it should be noted that the region where the wind veers (the southern tip of the excursion of high-PV air) includes the exit region of the jet streak going into the trough. Uccellini and Koch [1987], as well as Guest *et al.* [2000] insisted on the importance of the exit region of jet streaks propagating toward a ridge for gravity wave generation. The location of the radio soundings we used were too far south to account for the exit regions of the jet streaks propagating toward a ridge. We thus cannot compare the exit regions of the jet streaks propagating toward a ridge with those going toward a trough.

[37] The remaining 82 radio soundings were either ahead or behind the jet maximum, or in a flow without clearly identifiable pattern.

[38] The spatial distribution of the IGW intensity is different for the archetype flow patterns. The variation of  $A$  as a function of the distance to the jet is plotted in Figure 5 for each category of radio soundings separately. For the stratospheric slice, some specific features appear: the shift of the highest values of  $A$  toward the anticyclonic side is evident for the soundings near the maxima of the wind. For the soundings in the regions of strong jet curvature, the distribution of high  $A$  is more symmetric.

[39] The waves generated in the regions of maximal velocity of low-curvature jets may have multiple sources (shear instability, symmetric instability, surface frontogenesis, geostrophic adjustment). It is difficult to determine which mechanism is at the origin of the waves detected by the radiosoundings in these regions. On the other hand, in

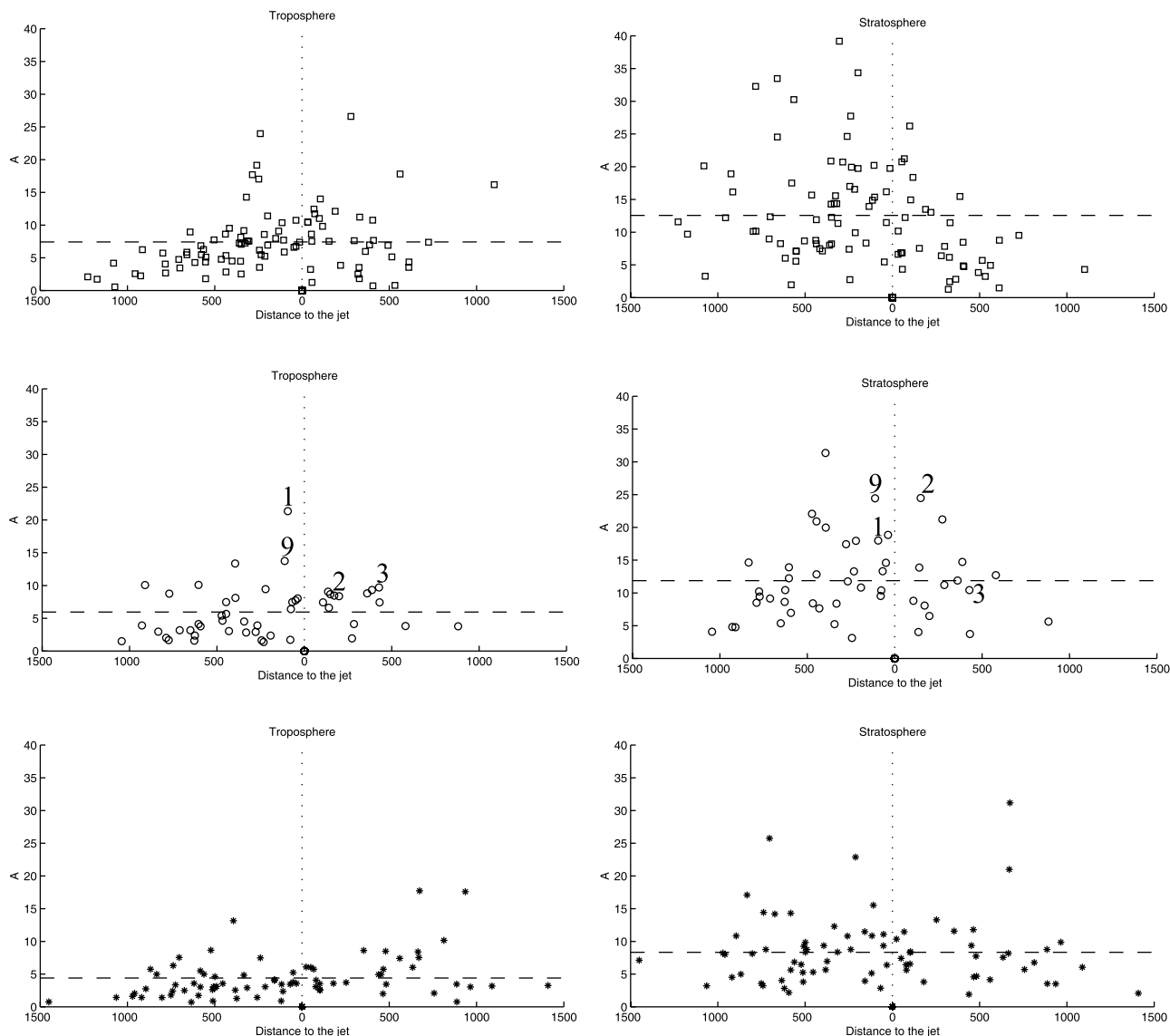


**Figure 5.** Distribution of the gravity wave activity  $A$  as a function of distance to the jet for each characteristic region of the flow: (top) the vicinity of the velocity maxima, (middle) the regions of strong curvature of the flow, and (bottom) the rest of the radio soundings. The average value of  $A$  for each category is indicated by a dashed line. Soundings 1, 2, 3, and 9, which are analyzed in the case studies of sections 4 and 5, are indicated in the middle row.

the regions of high curvature of the jet, radio soundings exhibiting a single clear-cut inertia gravity wave are frequently found. The detailed case studies presented below indicate that geostrophic adjustment of the jet is an important source for these waves. A first one is described in detail in section 4. A review of two other cases is given in section 5 illustrating further wave emission from the regions of highly distorted jet.

#### 4. A Case Study of the Geostrophic Adjustment

[40] In order to determine the generation mechanism and the characteristics of the waves observed in situations where the jet is severely distorted, we focus in the present section on six radio soundings which were launched on 5 and 6 February 1997, and which exhibit intense and coherent

inertia gravity wave activity in the lower stratosphere. Using the ECMWF data, we first analyze the synoptic situation and determine the regions of imbalance produced by the large-scale flow (subsection 4.1). The study of the waves detected by the radio soundings is presented in subsections 4.2 and 4.3. Finally, indications on the horizontal structure of the waves obtained from ECMWF analyses, using isentropic maps of the horizontal wind divergence, is given in section 4.4.

##### 4.1. Synoptic Situation on 5 and 6 February 1997

[41] During the 2 days of 5 and 6 February 1997, the jet was severely distorted exhibiting a V-like pattern, which travels across the Atlantic ocean in about 2 days (left column of Figure 6). This configuration of the flow can also be seen as a deep trough in the geopotential, or an

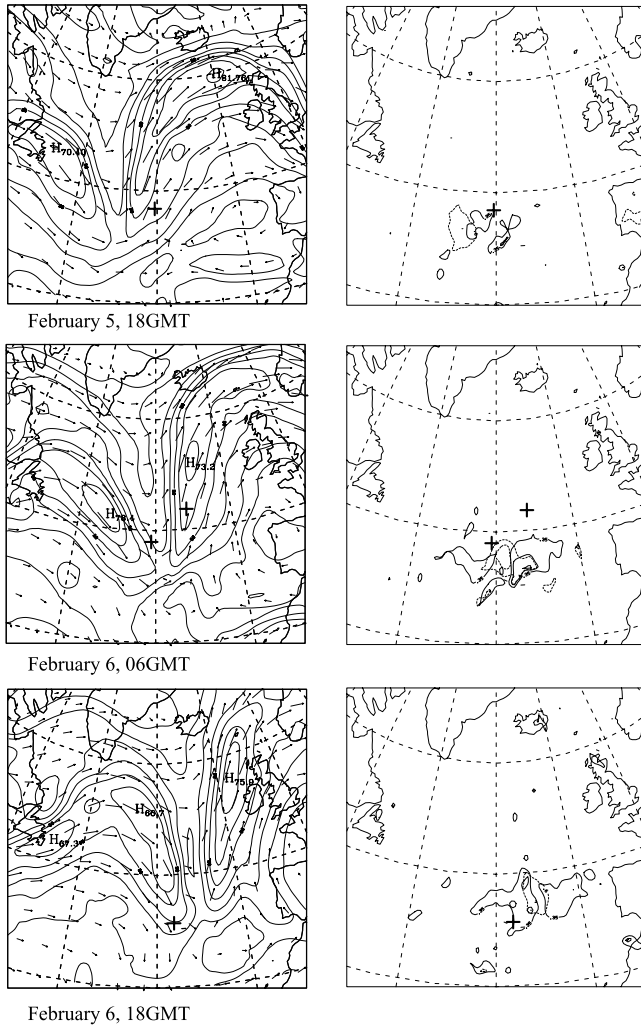


**Figure 6.** (left) Wind norm and velocity at  $Z = 8$  km (contours every  $10 \text{ ms}^{-1}$ ). (right) Lagrangian Rossby numbers at  $Z = 8$  km:  $Ro_{\perp}$  (solid line, threshold 0.35, contours every 0.2) and  $Ro_L$  (dashed line, threshold 0.6, contours every 0.3). Both  $Ro_{\perp}$  and  $Ro_L$  are presented only in regions where the wind speed exceeds the threshold of  $20 \text{ ms}^{-1}$ . (top) 5 February, 18:00 GMT. (middle) 6 February, 06:00 GMT. (bottom) 6 February, 18:00 GMT. The locations of the corresponding radio soundings are indicated by crosses: sounding 2 in the top panels, soundings 3 and 4 in the middle panels, and soundings 5 and 6 in the bottom panels.

equatorward excursion of the high-PV air on an isentropic surface (Figure 7), which corresponds to a breaking Rossby wave [cf. Hoskins *et al.*, 1985]. The region of high-PV air extending southward narrows down as it propagates eastward. By the end 7 February, it narrows further until a cut-off cyclone has formed off the coasts of Portugal and Morocco (not shown).

[42] In the tip of the V-shaped pattern which the jet follows on 5 and 6 February, the air parcels experience considerable Lagrangian accelerations (change of norm and change of direction, cf Figure 6). The flow becomes unbalanced in the regions where the Lagrangian acceleration becomes of the same order as the Coriolis force, i.e.,

where the Lagrangian Rossby number [Van Tuyl and Young, 1982],

$$Ro_L = \frac{|D\mathbf{v}/Dt|}{f|\mathbf{v}|} = \frac{|f\mathbf{v}_{ag} \times \mathbf{e}_z|}{f|\mathbf{v}|} = \frac{|\mathbf{v}_{ag}|}{|\mathbf{v}|}, \quad (2)$$

is of order 1. This criterion was used in studies of the generation of waves by the large-scale flow [O'Sullivan and Dunkerton, 1985; Reeder and Griffiths, 1996]. However, it will tend to overrepresent regions where the flow is close to a state of balance other than geostrophic balance (gradient wind balance), i.e., the regions where the jet is strongly curved. To correct this, Koch and Dorian [1988] introduced the cross-stream Lagrangian Rossby number  $Ro_{\perp}$ , defined using the component of the ageostrophic velocity perpendicular to the flow:

$$Ro_{\perp} = \frac{|\mathbf{v}_{ag}^{\perp}|}{|\mathbf{v}|}. \quad (3)$$

Indeed, as the gradient wind is parallel to the geostrophic wind, but differs in norm, part of the along-stream ageostrophic wind will account for the difference between the geostrophic and the gradient wind balance, and not for the overall flow imbalance.

[43] Zhang *et al.* [2000] have recently examined the relevance of these diagnostics using mesoscale numerical simulations. They have shown that  $Ro_L$  is indeed biased, whereas  $Ro_{\perp}$  is not, and is a reliable indicator of the unbalanced regions. As  $Ro_L$  is nevertheless commonly used, both are displayed in the right column of Figure 6. The Lagrangian Rossby numbers in Figure 6 were calculated only in regions where  $|\mathbf{v}| > 20 \text{ ms}^{-1}$ , and contours were plotted only for  $Ro_L > 0.6$  and  $Ro_{\perp} > 0.35$ . These thresholds are chosen so that Figure 6 indicates the most significant regions. (Note that the velocity maxima of the jet never correspond to high values of the Lagrangian Rossby numbers, although ageostrophic circulations may be important there.) The Lagrangian Rossby number  $Ro_L$  typically exhibits a regular-shaped maximum at the tip of the V pattern, where the curvature of the wind is strongest and the norm of the wind is moderate (around

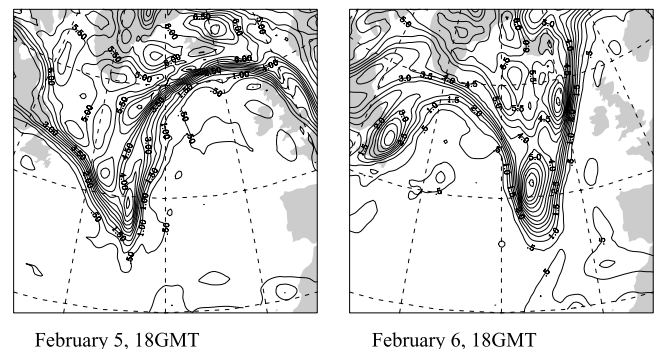


**Figure 7.** Potential vorticity on the 310 K isentropic surface on (left) 5 February, 18:00 GMT and (right) a day later, on 6 February, 18:00 GMT.

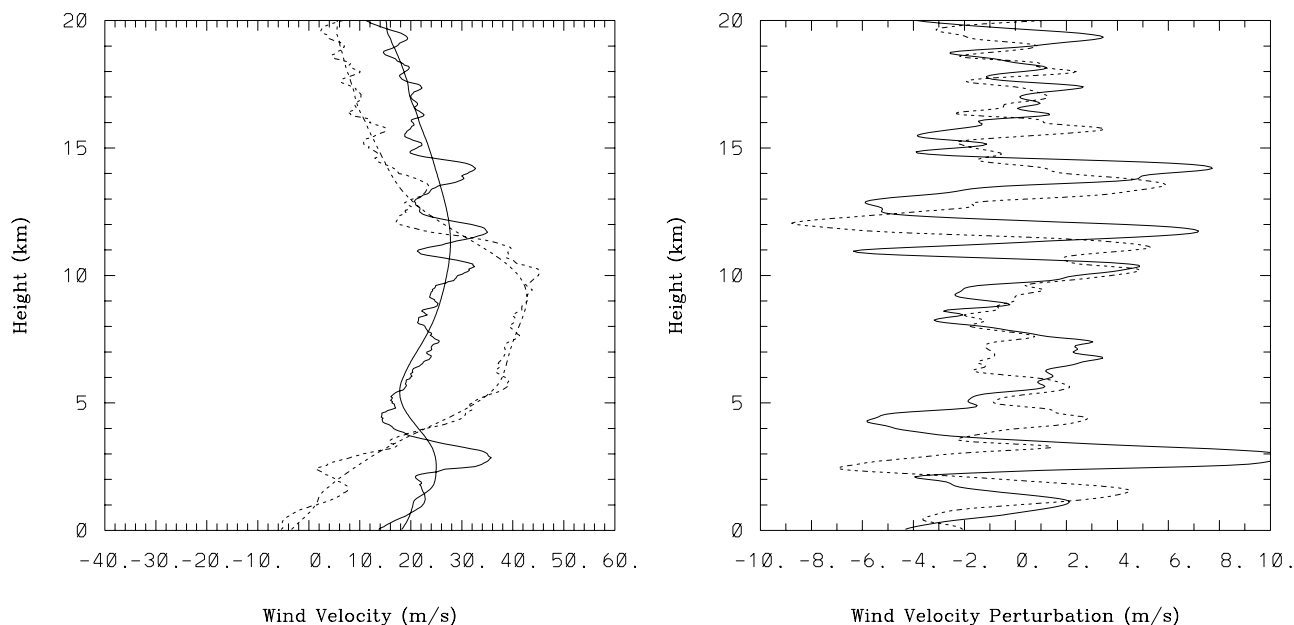


**Figure 8.** Vertical profiles of the wind and the wind disturbance for radio sounding 1, launched from the ship *Victor Bugaev* on 5 February, 11:30 GMT. (left) Total and background velocities; the zonal (solid line) and meridional (dashed line) components are displayed. (right) Disturbance wind obtained by filtering out the scales larger than 5 km or shorter than 300 m. The corresponding hodograph is shown in Figure 9.

$30 \text{ ms}^{-1}$ ). In the present case, there are two maxima of  $Ro_{\perp}$ , upstream and downstream of the maximum of  $Ro_{\parallel}$ , corresponding to the exit region of the southeastward jet streak and to the entry region of the northeastward jet streak (compare Figures 6b and 6c). It will be seen from the radio soundings that IGW are detected in both of these regions.

#### 4.2. Inertia Gravity Waves Observed in Radio Soundings Launched From the Ships on 5 and 6 February

[44] We present below the analysis of a lower-stratospheric wave observed in four radio soundings launched from ships between 5 February, 11:30 GMT, and 6 February, 09:30 GMT and located at the limit or just downstream of the region of flow imbalance outlined in the previous section. For each sounding, the vertical profile of the wind disturbance and the hodograph are displayed (Figures 8 and 9 for sounding 1, Figure 10 for sounding 2, Figures 11 and 12 for sounding 3, Figure 13 for sounding 4). The vertical wavelength of the waves is determined from these data, and the wave's intrinsic frequency, horizontal wavelength and the orientation of the wave vector are estimated.

[45] The location and time of the radio soundings are given in Table 1. The first two of them were located on the border of the unbalanced region as defined by  $Ro_{\perp}$  (not shown for sounding 1, see Figure 6 for soundings 2 and 3). This corresponds to the entry region of the northeastward jet streak (see the wind profile in Figure 8), after the wind veered. The radio soundings 1 and 2 are located downstream of the unbalanced region. The third radio sounding is in the region of weak winds inside the V pattern (see the wind profile in Figure 11). The fourth

sounding is located a bit further downstream, in the northeastward branch of the jet (its location is indicated in Figure 6, using the analysis for 6 February, 06:00 GMT; however, given the time of launching and the duration of the ascent, it is preferable to locate it relative to the flow using the analysis for 12:00 GMT: the

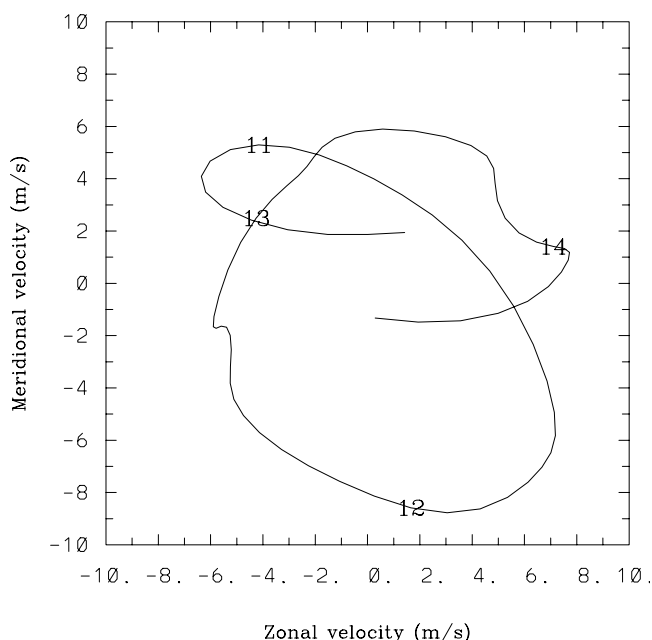


**Figure 9.** Hodograph for the sounding launched from the ship *Victor Bugaev* on 5 February, 11:30 GMT, in the height interval 10.5–14.5 km, as obtained from the disturbance velocities displayed in Figure 8.

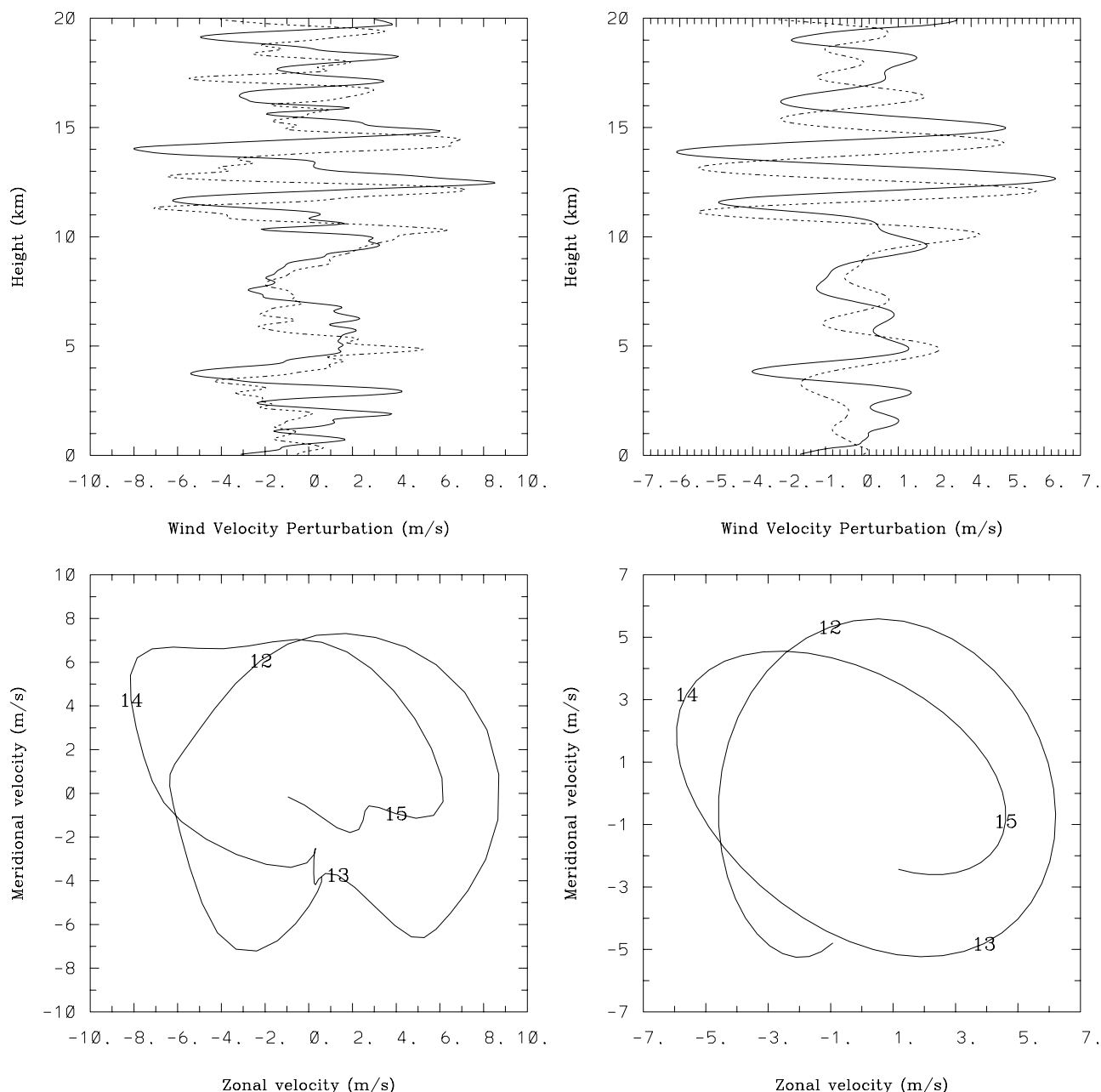


**Figure 10.** Velocity profile and hodograph (11–15.5 km) of the wind perturbation detected in sounding 2, launched from the ship *Le Suroit* on 5 February, 20:31 GMT. (left) The disturbance velocity obtained by filtering out the scales larger than 5 km and shorter than 300 m. (right) In order to illustrate the use of additional filtering to determine the wave parameters, the profile obtained by filtering out the scales larger than 4 km and smaller than 1.5 km (see Table 2) is shown.

sounding is then seen on the western side of the northward branch of the jet).

[46] All of the four radio soundings exhibit an intense and coherent inertia gravity wave in the lower stratosphere (from 10 to 15 km). As this feature appears very clearly and with comparable characteristics in the six soundings analyzed for this event, we will refer to it as “the wave”, although it is more exact to say that we observe a (rather narrow) wave packet. The anticyclonic rotation of the hodographs shows that the energy is propagating upward (Figures 9, 10, 12, and 13); the aspect ratio of the ellipses

in the hodograph is close to 1, indicating that a low-frequency wave is observed. A sign of downward propagation of IGW can also be seen in the lower troposphere (1–5 km) for soundings 1 and 3 as inversion of the lag between the two components of velocity (see vertical profiles of wind disturbance in Figures 8 and 11), indicating that the source of the waves is indeed the upper tropospheric jet.

[47] If the aspect ratio  $R$  and the vertical wavelength  $\lambda_z$  of a given quasi-monochromatic wave are known, the frequency ( $\omega = f/R$ ) of the wave and its horizontal wavelength  $\lambda_H$  may

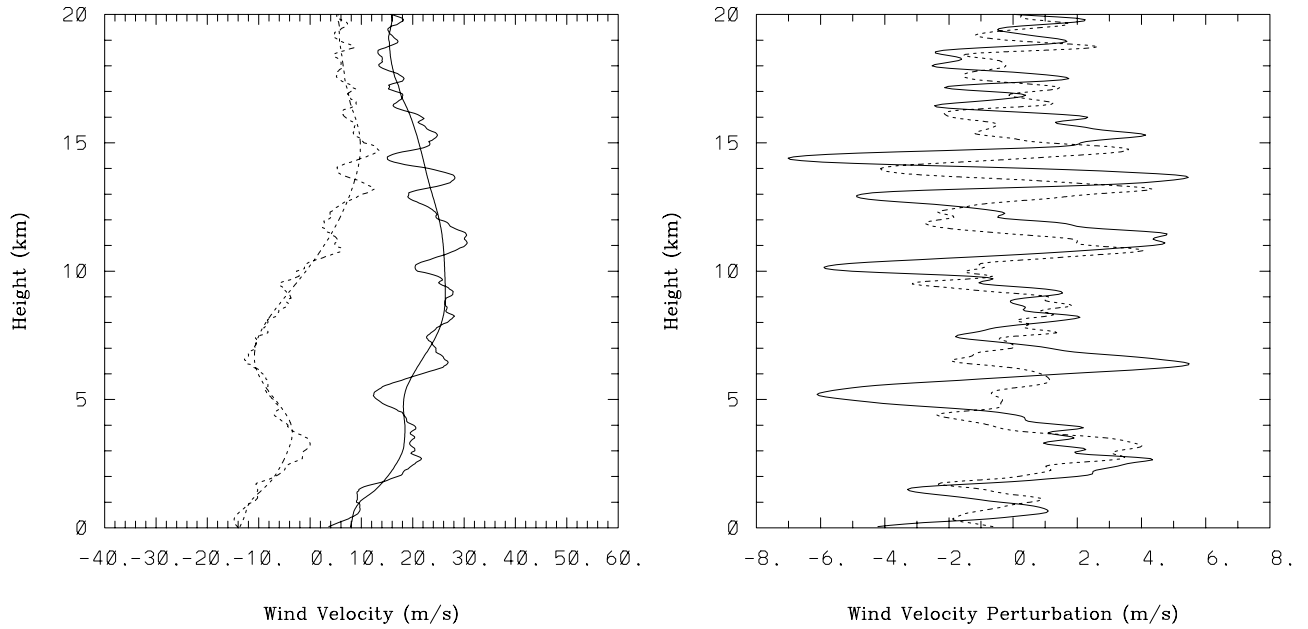


**Figure 11.** Wind and wind disturbance profiles for the radio sounding launched from the ship *Le Suroit* on 6 February, 05:36 GMT.

be estimated from the linear dispersion relation for hydrostatic waves:

$$\omega^2 = f^2 + \frac{N^2 \lambda_z^2}{\lambda_H^2}. \quad (4)$$

[48] For the determination of the characteristics of the wave, the fact that the sonde does not provide an instantaneous vertical profile can be a matter of concern: indeed, it is horizontally advected by the wind as it ascends through the wave region (displacement of order 30 km), and takes a certain time to ascend through the wave (the ascent velocity is typically  $5 \text{ ms}^{-1}$ ). Analyzing the velocity profiles as vertical is justified if the horizontal displacements are small relative to the wavelength, and the time dependence of the data can be safely neglected if the time of ascent through a vertical wavelength is small relative to the intrinsic period [Guest *et al.*, 2000]. In the present case, both conditions are verified.

[49] In order to determine more precisely the vertical wavelength of the detected wave and its aspect ratio (that of the ellipses in the hodographs), the observed profiles have been filtered using an adaptive window which was defined after preliminary examination of the Fourier transforms of the profiles. The windows and the wave parameters thus obtained are listed in Table 2. The aspect ratio is not always well defined; an example of this ambiguity is shown for the velocity profiles and hodograph in Figure 10. The aspect ratio was measured within the altitude range where the wave was most intense. For the lower-stratospheric wave observed in these four radio soundings, the aspect ratio is approximately 0.7, though for the second and fourth soundings it may be higher.

[50] The location of the maximum wave activity, the vertical wavelength and the aspect ratio are almost the same in the four radio soundings, indicating that it is the same

wave that is observed in all four of them. Its amplitude is stronger in the second radio sounding; the wave is weaker but most unambiguously defined in the third; this sounding is farther from the region of large-scale imbalance indicated by the analyses, which may explain why the wave amplitude there is smaller, and the background wind and shear are weaker. This may explain, in turn, why the ellipse in the hodograph (Figure 12) is so neat. The wave’s intrinsic frequency being low, its group velocity is small, and the

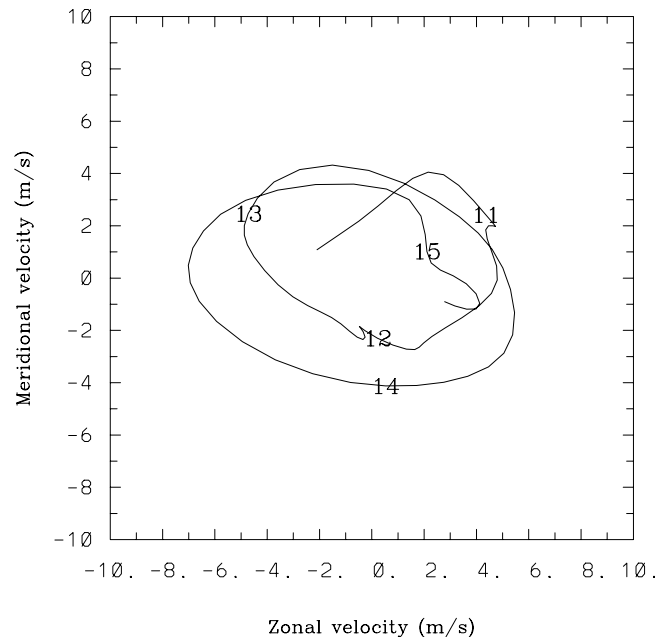


**Figure 12.** Hodograph (10.5–15.5 km) for sounding 3, launched from the ship *Le Suroit* on 6 February, 05:36 GMT.

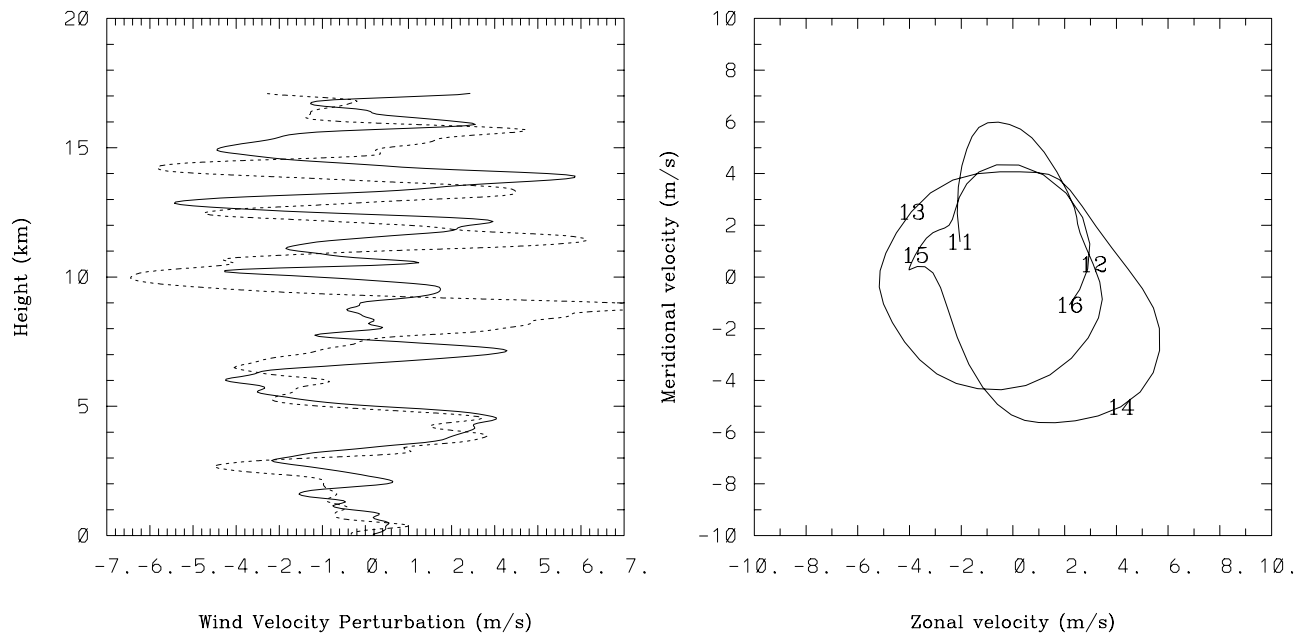


**Figure 13.** Wind disturbance profile and hodograph for sounding 4, launched from the ship *Aegir* on 6 February, 09:25 GMT.

wave is expected to be advected by the jet. This is consistent with the observation of the wave further downstream in sounding 4.

[51] The Brunt-Vaisala frequency was calculated from the temperature measurements of the soundings, and was found to be  $2.1 \times 10^{-2} \text{ s}^{-1}$  in the lower stratosphere. Taking the typical aspect ratio to be 0.7 we estimate the intrinsic period and the horizontal wavelength of the wave detected in the three radio soundings as  $\sim 12$  hours and 400–450 km, respectively.

[52] The orientation of the wave vector can be determined from the direction of the major axis of the hodograph’s ellipse. Its direction can then be estimated from the profiles of potential temperature obtained from the measurements of temperature and pressure. This analysis shows the wave vector pointing to northwest in the first two and the fourth radio soundings, and pointing to WNW in the third radio sounding. Hence the wave vector in the radio soundings 1, 2 and 4 is transverse to the mean flow in the northeastward branch of the jet.

[53] The remarkable agreement of the characteristics of the wave in the four soundings, the fact that the wave is large scale and low frequency, and is observed close to the region of imbalance diagnosed from the ECMWF analyses are evidence that the wave is generated by geostrophic adjustment of the jet. The stratospheric wave (energy flux upward) is much more clearly identified than the tropospheric one (energy flux downward), yet both are detected.

**4.3. Inertia Gravity Waves Observed on 6 February in Two Radiosoundings Launched From the Azores Islands**

[54] We present below the evidence that the IGW generation by geostrophic adjustment in the region of strong flow curvature is continuing about 1 day later, as the trough was propagating over the Atlantic. We use two radio soundings that were launched from Lajes in the Azores Islands on 6 February. Their resolution is only of about 250 m, and hence they were not used for the statistical analysis of section 3.

**Table 1.** Time and Location of the Launches of Radio Soundings<sup>a</sup>

Sounding No.	Location	Day	GMT, h:min	Longitude, deg	Latitude, deg	<i>A</i> (Stratosphere)
<i>5–6 February 1997</i>						
1	<i>Victor Bugaev</i>	5	11:30	–37.45	+41.28	18.0
2	<i>Le Suroit</i>	5	20:31	–30.45	+42.79	24.5
3	<i>Le Suroit</i>	6	05:36	–30.85	+43.64	10.4
4	<i>Aegir</i>	6	09:25	–34.45	+41.03	16.3 <sup>b</sup>
5	Azores	6	17:19	–27.1	+38.7	
6	Azores	6	23:24	–27.1	+38.7	
<i>11 February 1997</i>						
7	<i>Victor Bugaev</i>	11	17:30	–35.0	+40.8	
8	Azores	11	23:24	–27.1	+38.7	
<i>22 February 1997</i>						
9	<i>Victor Bugaev</i>	22	11:30	–34.45	+41.03	24.4

<sup>a</sup>The last column indicates the gravity wave activity *A* (in  $\text{m}^2 \text{s}^{-2}$ ) in the stratosphere in these soundings.

<sup>b</sup>Calculated only for heights going from  $z = 12$  km to the end of the sounding at  $z = 17.1$  km.

**Table 2.** Characteristics of the Waves Observed in the Lower Stratosphere in Radio Soundings<sup>a</sup>

Sounding No.	Height, km	$\lambda_z$ , km	Window, km	Aspect Ratio	$ \mathbf{u}'_{\max} $ , $\text{ms}^{-1}$
<i>5–6 February 1997</i>					
1	10.5–14.5	2.2	1.5–5	0.7	8
2	10.5–15	2.2	1.5–4	0.7–0.9	9
3	9–15.5	2.1	1.5–3	0.7	7
4	11–16	1.9	1–5	0.7–1	6
5	9.5–15	2.4	1–3.5	0.35	7
6t	1–5	2.3	1.5–4	0.5	4
6s	9–14	2.5	1.5–4	0.5–0.65	7
<i>11 February 1997</i>					
7	1–6	2.5	0.1–5	0.4–0.6	4
8t	3–9	2.3	0.1–5	0.5–0.7	7
8s	11–16	2	0.1–5	0.6	7
<i>22 February 1997</i>					
9t	3–8	2.7	0.5–5	0.15	7
9s	12–19	1.9	0.5–5	0.5–0.75	9

<sup>a</sup>The columns contain, successively, the radio sounding number, the height range in which the wave is unambiguously detected, the vertical wavelength, the adaptive window used to determine the aspect ratio, the aspect ratio itself, and the order of magnitude of the maximum wave velocity.

[55] The soundings were launched in the exit region of the southeasterly jet streak, to the south of the unbalanced region identified in Figure 6. The precise location and time of launch of the soundings is given in Table 1.

[56] In radio sounding 5 an intense ( $\sim 7 \text{ ms}^{-1}$ ) wave of rather low frequency was observed in the lower stratosphere (10–15 km). Indications for a wave propagating downward in the troposphere (3–7 km) are also present (not shown). The generation at the level of the jet is clearer in radio sounding 5: in the velocity perturbation (Figure 14), one can see the characteristic shift between the maxima of  $u'$  and  $v'$

indicating downward propagation of energy in the troposphere and upward propagation in the stratosphere. The corresponding hodographs (Figure 15) display, respectively, cyclonic and anticyclonic rotation.

[57] The characteristics of the waves are displayed in Table 2. For the lower stratospheric wave, they are similar to the ones obtained from the soundings 1–4. This and the persistence of the large-scale imbalance at the tip of the trough in the ECMWF analyses suggests that this region of the flow acts as a continuous source of IGW, mostly for the lower stratosphere, but also for the troposphere. In their numerical simulations, *O'Sullivan and Dunkerton [1995]* had indeed found that an IGW packet was approximately stationary relative to the jet exit region; in these simulations however, no IGW generation in the troposphere was observed. In the subsequent studies of IGW generation from regions of jet distortion, *Thomas et al. [1999]* have also observed waves generated at the jet and propagating both into the stratosphere and into the troposphere, but with smaller amplitudes ( $2 \text{ ms}^{-1}$ ).

#### 4.4. Remarks on the Horizontal Structure of the Waves From the Horizontal Divergence in the ECMWF Analyses

[58] In spite of the known uncertainties as to the IGW generation, the ECMWF analyses may give some qualitative indications of the horizontal structure of the waves, which can be inferred from the maps of the divergence of the horizontal wind on isentropic surfaces. Isentropic maps of the divergence of the horizontal wind obtained from ECMWF analyses have already been used for studying large-scale inertia gravity waves by *Moldovan et al. [2002]*. Although we cannot expect that the ECMWF give a quantitatively accurate description of a wave with a vertical wavelength of 2 km (the resolution at which the

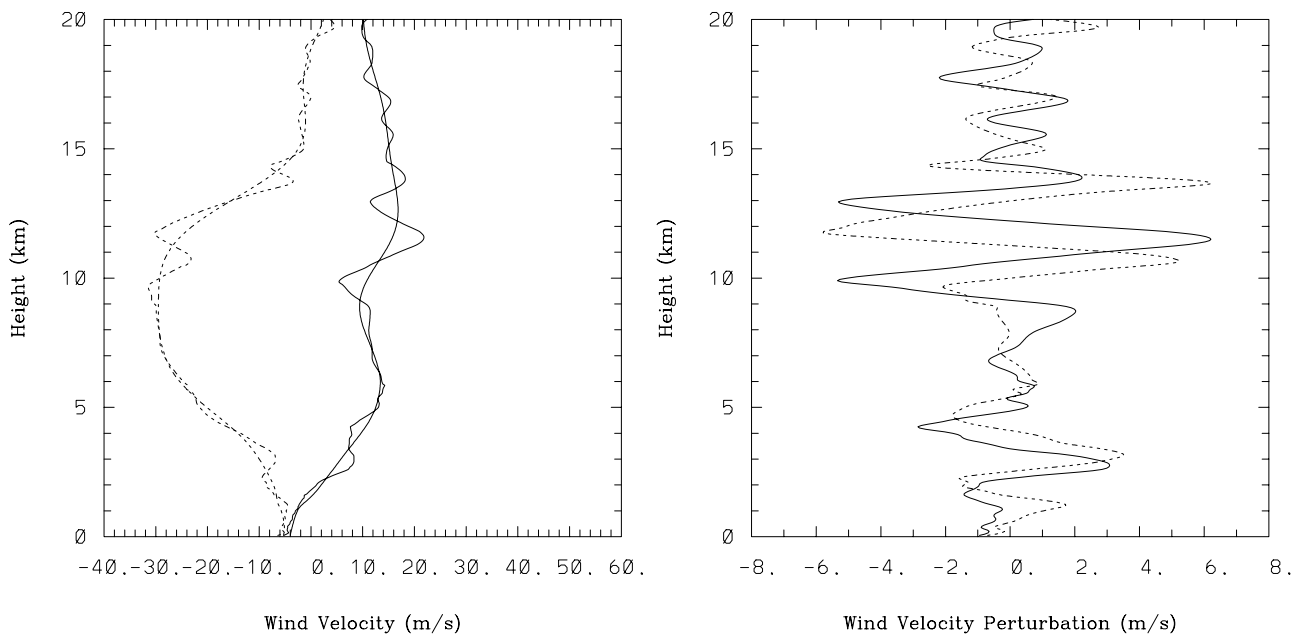


**Figure 14.** Wind velocity and wind disturbance for radio sounding 6, launched from the Azores on 6 February, 23:24 GMT.

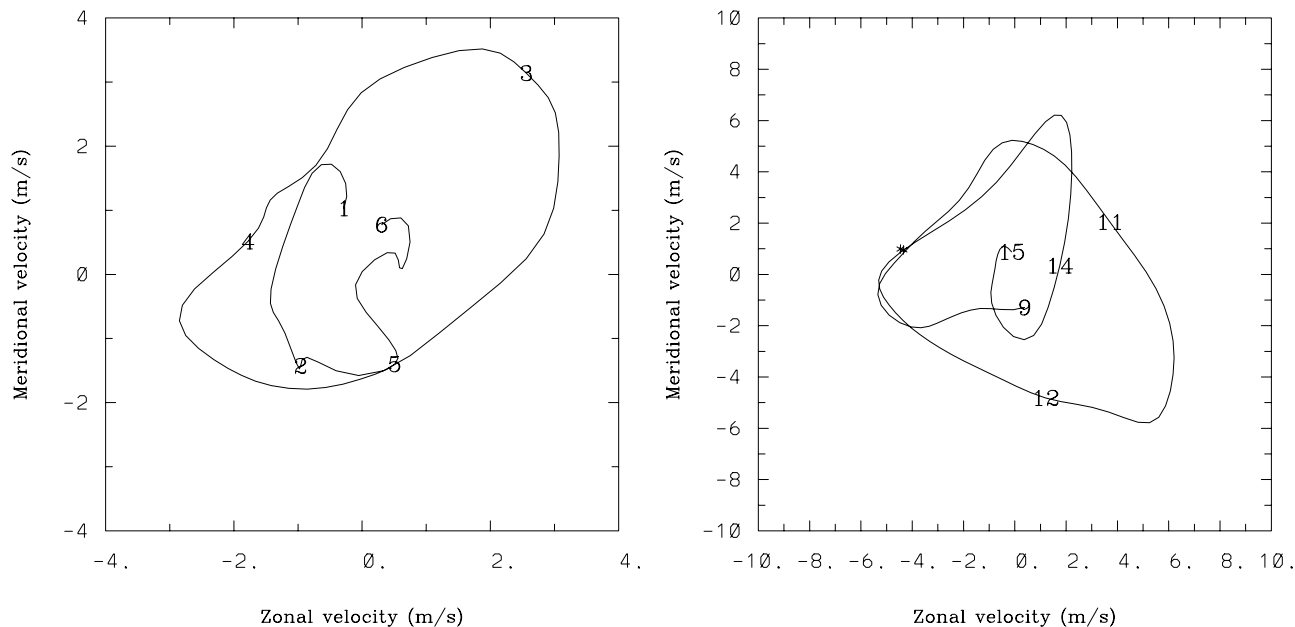


**Figure 15.** Hodographs for radio sounding 6, launched from the Azores on 6 February, 23:24 GMT. (left) Tropospheric hodograph (1–6 km); the cyclonic rotation indicates the downward propagation of energy. (right) Stratospheric hodograph (9–15 km); the anticyclonic rotation corresponds to energy propagating upward.

ECMWF model is run is of about 50 km in the horizontal, with 60 levels in the vertical up to 1 hPa and 15 min time step), we can expect that, as the model does describe the generation of a region of large-scale imbalance during evolution of the jet, it will contain some waves produced by the geostrophic adjustment of this region. The waves may not have the correct wavelengths and frequencies, but the time and location of their generation are expected to be relevant [Plougonven and Teitelbaum, 2003]. This reasoning is supported by the tests made by O’Sullivan and Dunkerton [1995] on the effect of resolution on IGW generation [O’Sullivan and Dunkerton, 1995, Figure 9].

[59] The maps of the divergence of the horizontal wind on isentropic surfaces obtained from the ECMWF analyses for the dates of interest are presented in Figure 16. We observe that the location of the waves and their orientation as seen

on the maps are consistent with what the soundings suggest. This is an element of confirmation of our interpretation of the soundings data.

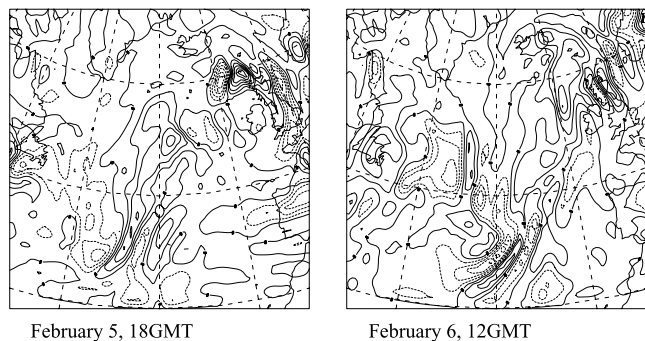


**Figure 16.** Maps of the divergence of the horizontal wind on the isentropic surface 340 K as given by the ECMWF analyses: (left) 5 February, 18:00 GMT; (right) 6 February, 12:00 GMT. Clear wave-like patterns of alternating convergence and divergence are present in both maps in the exit region of the southeastward jet streak.

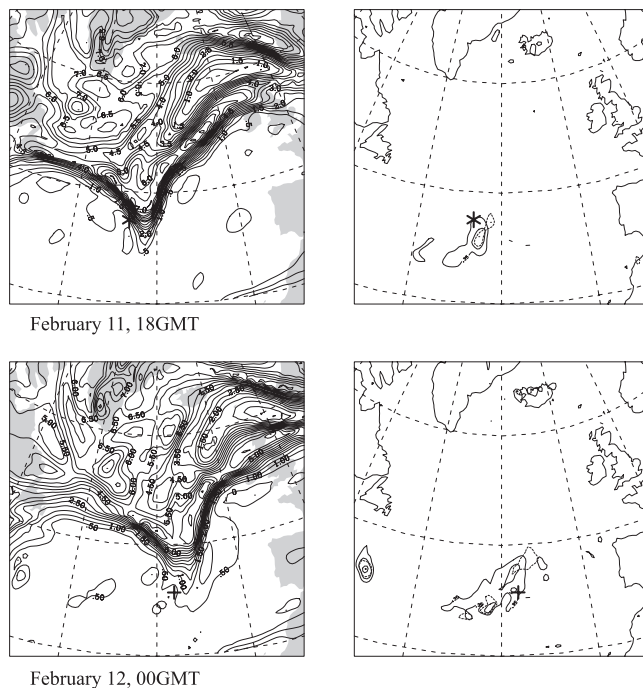


**Figure 17.** (left) Potential vorticity on the isentropic surface 320 K and (right) the Lagrangian Rossby numbers on the isobaric surface  $Z = 8$  km. The contour intervals for the Rossby Lagrangian are as in Figure 6. (top) 11 February, 18:00 GMT, indicating the location of sounding 7 (asterisk). (bottom) 12 February, 00:00 GMT, indicating the location for sounding 8.

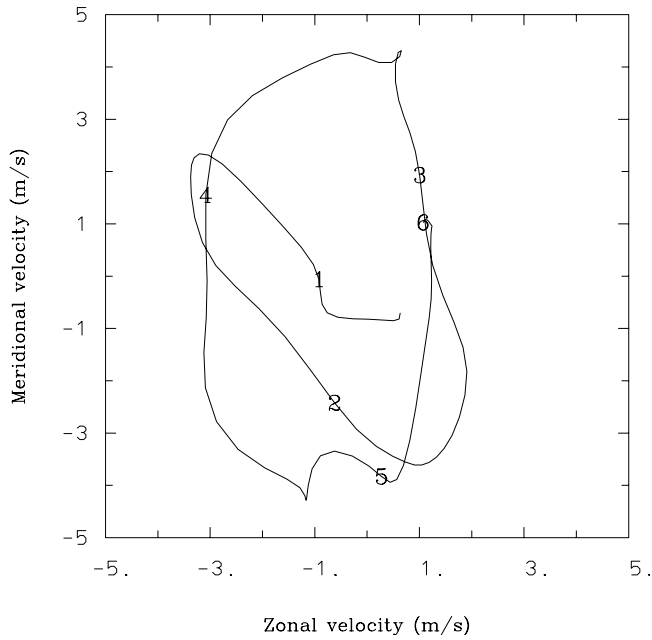


**Figure 18.** Hodograph (1–6 km) for the radio sounding launched from the ship *Victor Bugaev* on 11 February, 17:30 GMT, in the window 300 m to 5 km. The cyclonic rotation indicates the downward propagation of energy. No hodograph is displayed for the lower stratosphere because the vertical profiles of the velocity did not extend beyond about 6.7 km.

[60] The maps suggest that the waves are generated primarily in the exit region of the southeasterly jet streak, where the wind veers toward the northeast. The orientation of the phase lines are consistent with the northwest orientation found for the wave vector in subsection 4.2. In the jet

exit region of the southeasterly jet streak, this corresponds to the wave vector parallel to the jet, and oriented upstream, which is consistent with what *O’Sullivan and Dunkerton* [1995] found in their numerical simulations.

**5. Comparison to Other Similar Events**

[61] In section 3, the regions where the flow is highly curved were shown to favor intense IGW activity. In the previous section, a case study showed that the IGW activity observed in such regions was due to the emission, through geostrophic adjustment, of large-amplitude, large-scale IGW. The related configuration of the jet (distorted toward the south, corresponding to a trough in the upper-tropospheric geopotential) is recurrent [*Hoskins et al.*, 1985]. In the present section, we analyze briefly two cases of IGW emission from similar configurations of the jet, with respectively weaker and stronger deformation, to show that the process of geostrophic adjustment in such configurations appears in a systematic way.

**5.1. A Case With a Weaker Deformation of the Jet: 11 February**

[62] On 11 February, the configuration of the jet is similar to that of 5 and 6 February, though the jet distortion is weaker. Here again, there is a deformation of the jet that can be attributed to a Rossby wave, with an unbalanced region corresponding to the extremity of the equatorward excursion of the high-PV air (Figure 17; note that in this example, where the curvature of the flow is less important, the maxima of both Lagrangian Rossby numbers generally coincide).

[63] Two radio soundings were launched in the region of unbalanced flow. Their precise locations are given in Table 1. The velocity measurements in radio sounding 7 go up only to 6.7 km. It nevertheless reveals an intense tropospheric inertia gravity wave with energy propagating

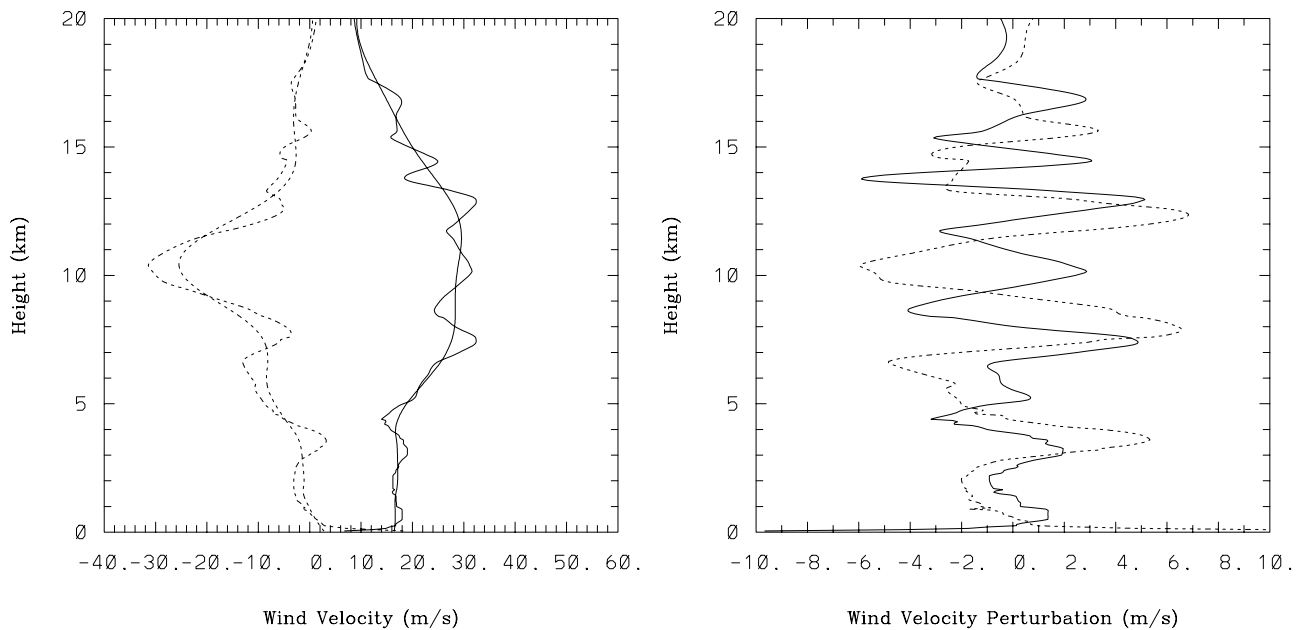
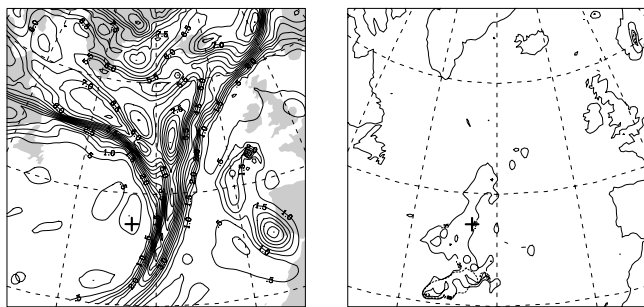


**Figure 19.** Wind profile and perturbation velocity for the radio sounding from the Azores Island, 11 February, 23:24 GMT. The relative positions of the maxima of  $u'$  and  $v'$  show IGW with downward energy propagation in the troposphere and with upward energy propagation in the lower stratosphere.



February 22, 12GMT

**Figure 20.** Potential vorticity on isentropic surface 320 K and the Lagrangian Rossby numbers on isobaric surface  $Z = 6$  km for 22 February, 12:00 GMT, as in Figure 17. The location of sounding 9 is indicated by a cross.

downward in the altitude range 1–6 km. The hodograph of the wind disturbance is shown for this sounding in Figure 18. The vertical wavelength is approximately 2.5–3 km, and the aspect ratio is approximately 0.5; the horizontal wavelength is hence estimated to be approximately 170 km.

[64] Sounding 8 was launched from the Azores Island. The profiles of the wind and of the wind disturbance are shown in Figure 19: the generation of a tropospheric and a stratospheric IGW at the level of the jet (around 10 km) is evident and can be inferred from the inversion of the lag between the two velocity components. As can be seen from Table 2, the wave characteristics are comparable to those found in sounding 7.

[65] The divergence of the horizontal wind field on isentropic surfaces, from ECMWF analyses (not shown), displays again, as for 5 and 6 February, some typical IGW structures downstream of the region of imbalance. The

phase lines are again approximately parallel to the north-eastward branch of the jet.

### 5.2. A Case With a Stronger Deformation of the Jet: 21 and 22 February

[66] As the last example, we show below the evidence of the IGW generation by the geostrophic adjustment on 21–22 February 1997 when the jet was severely distorted. The deformation of the jet in this case is greater than on 5 and 6 February (Figure 20). An extended region of imbalance of the flow is present; its location, however, slightly differs compared to the case of 5 and 6 February: the imbalanced domain is situated in the exit region of the jet streak propagating toward the trough, i.e., on the western side of the equatorward excursion of the high-PV air.

[67] A radio sounding was launched from the ship *Victor Bugaev* on 22 February within the exit region of the jet streak (see Figure 20). Intense gravity wave activity can be seen in the profile of the wind disturbance (see Figure 21). The hodographs (Figure 22) show a downward propagating tropospheric wave below the jet, and upward propagating wave activity above. This measurement again shows that the jet is the wave source.

## 6. Summary and Discussion

[68] Thus, using a sample of 224 radio soundings launched from the ships in the North Atlantic during the FASTEX campaign in February 1997, we identified the IGW contributions to the measured wind profiles and studied the intensity of the IGW activity as a function of the distance to the jet. Analyses from the ECMWF were used to locate the jet on the maps of the norm of the velocity at the log pressure level  $Z = 9$  km. We found that the distributions of the wave activity were centered near the jet axis, both in the stratosphere and troposphere, indicating

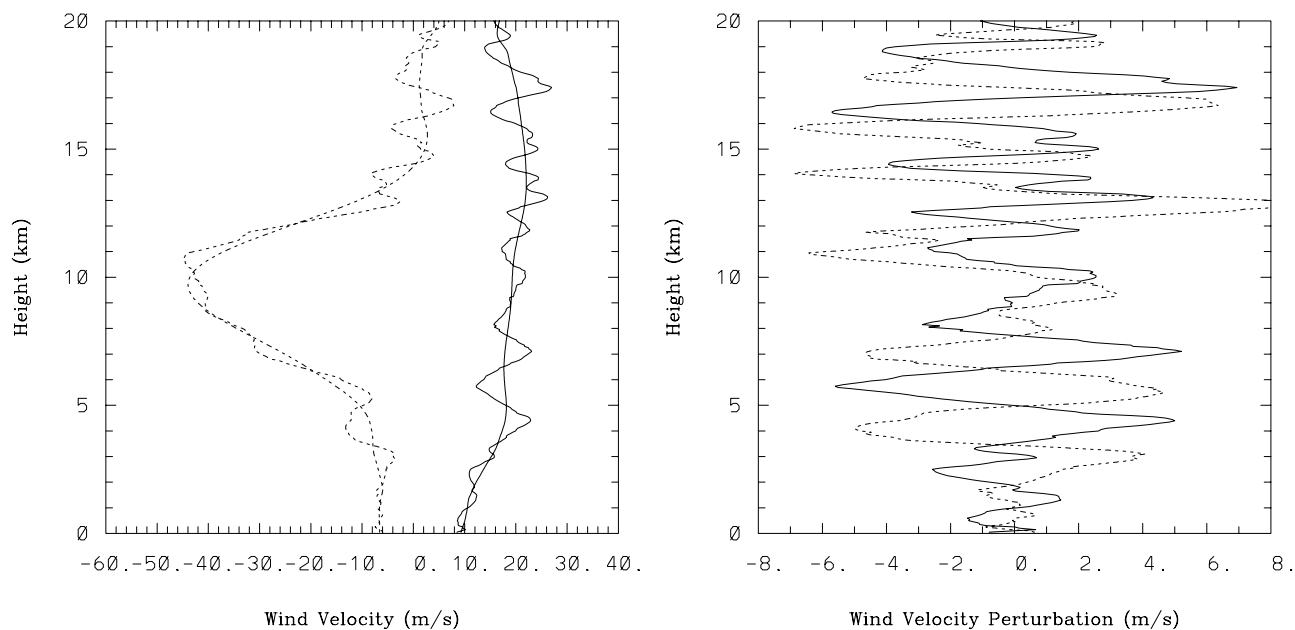


**Figure 21.** Profiles of the wind velocity and disturbance for sounding 9, launched from the ship *Victor Bugaev* on 22 February, 11:30 GMT.

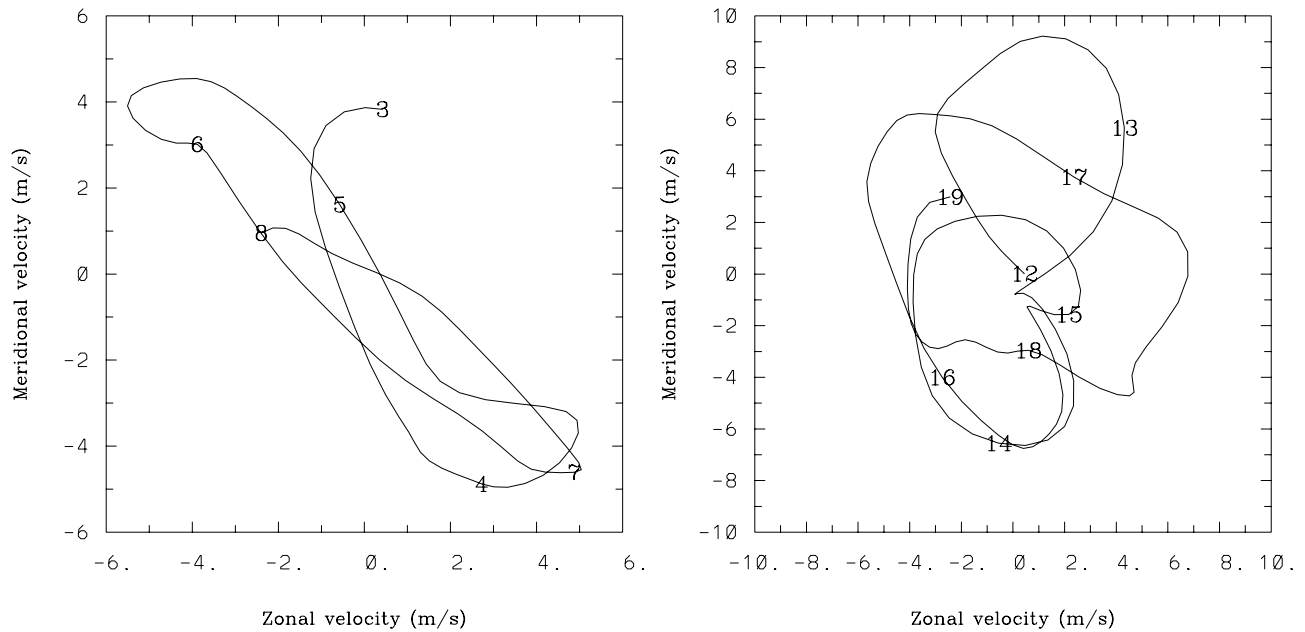


**Figure 22.** (left) Tropospheric (3–8 km) and (right) stratospheric (12–19 km) hodographs for sounding 9, launched from the ship *Victor Bugaev* on 22 February, 11:30 GMT.

that the jet is the dominant source of gravity waves far from orography.

[69] Closer inspection revealed that the radio soundings with the highest wave activities were situated in two specific regions of the flow: the vicinity of the jet velocity maxima and the regions of high curvature of the jet. The distribution of the wave activity as a function of the distance to the jet differs in the two cases. In the regions of high curvature of the flow this distribution is almost symmetric about the jet axis. In the vicinity of the jet velocity maxima, the peak of the distribution is shifted toward the cyclonic side of the jet in the troposphere (although, due to the undersampling of the cyclonic part of the jet the statistical relevance of this pattern is not sure), while in the lower stratosphere the soundings with the highest wave activity are located at the anticyclonic side of the jet, with the maximum of the distribution at about 300 km from the jet.

[70] The detailed case studies suggest that in the regions of the high curvature of the jet geostrophic adjustment is the mechanism producing the observed waves. The waves thus generated are intense, large-scale inertia gravity waves with vertical wavelengths typically between 2 and 3 km, and with frequencies, estimated by the hodograph method, typically between  $f$  and  $2f$ . Because they are due to the evolution of the large-scale flow, the analyses of the ECMWF can provide qualitative indications of their horizontal structure and location on the maps of the divergence of the horizontal wind on isentropic surfaces.

[71] Our observations are, in general, in agreement with the numerical simulations of this generation mechanism by *O’Sullivan and Dunkerton* [1995], but there are nevertheless some differences. First, the generation region in our case studies is located deeper in the trough of geopotential, near the exit region of the jet streak going toward the trough, where the wind veers. This is consistent with the

results of [*Hertzog et al.*, 2001], who found the origin of the IGW they observed near the tip of an equatorward excursion of the high-PV air, on its western flank. Second, the waves generated by the jet were present in the numerical simulations of *O’Sullivan and Dunkerton* [1995] only in the lower stratosphere. In several cases displayed above, the radio soundings clearly contained a tropospheric IGW with energy propagating downward out of the jet, as far down as 1 km above the sea level. *Thomas et al.* [1999] have also observed that the geostrophic adjustment of the jet was producing both stratospheric and tropospheric waves. In our observations, the tropospheric waves were generally less neat as compared to their stratospheric counterparts, with smaller amplitudes, which could nevertheless reach  $6 \text{ ms}^{-1}$ .

### References

Andrews, D. G., J. R. Holton, and C. B. Leovy, *Middle Atmosphere Dynamics*, Academic, San Diego, Calif., 1987.  
 Blumen, W., Geostrophic adjustment, *Rev. Geophys.*, 10, 485–528, 1972.  
 Blumen, W., and R. Wu, Geostrophic adjustment: Frontogenesis and energy conversion, *J. Phys. Oceanogr.*, 25, 428–438, 1995.  
 Bühler, O., M. E. McIntyre, and J. F. Scinocca, On shear-generated gravity waves that reach the mesosphere. part I: Wave generation, *J. Atmos. Sci.*, 56, 3749–3763, 1999.  
 Ciesielski, P. E., D. E. Stevens, R. H. Johnson, and K. R. Dean, Observational evidence for symmetric instability, *J. Atmos. Sci.*, 46, 817–831, 1989.  
 Danielsen, E. F., R. S. Hipskind, W. L. Starr, J. F. Vedder, S. E. Gaines, D. Kley, and K. K. Kelly, Irreversible transport in the stratosphere by internal waves of short vertical wavelength, *J. Geophys. Res.*, 96, 17,433–17,452, 1991.  
 Dunkerton, T. J., Inertia-gravity waves in the stratosphere, *J. Atmos. Sci.*, 41, 3396–3404, 1984.  
 Eckermann, S. E., and R. A. Vincent, VHF radar observations of gravity-wave production by cold fronts over southern Australia, *J. Atmos. Sci.*, 50, 785–806, 1993.  
 Fovell, R., D. Durran, and J. R. Holton, Numerical simulations of convectively generated stratospheric gravity waves, *J. Atmos. Sci.*, 49, 1427–1442, 1992.  
 Fritts, D. C., Shear excitation of atmospheric gravity waves, *J. Atmos. Sci.*, 39, 1936–1952, 1982.

- Fritts, D. C., and Z. Luo, Gravity wave excitation by geostrophic adjustment of the jet streams, part I: Two-dimensional forcing, *J. Atmos. Sci.*, *49*, 681–697, 1992.
- Fritts, D. C., and G. D. Nastrom, Sources of mesoscale variability of gravity waves. part II: Frontal, convective, and jet stream excitation, *J. Atmos. Sci.*, *49*, 111–127, 1992.
- Gall, R. L., R. T. Williams, and T. L. Clark, Gravity waves generated during frontogenesis, *J. Atmos. Sci.*, *45*, 2204–2219, 1988.
- Garner, S. T., Fully Lagrangian numerical solutions of unbalanced frontogenesis and frontal collapse, *J. Atmos. Sci.*, *46*, 717–739, 1989.
- Griffiths, M., and M. J. Reeder, Stratospheric inertia-gravity waves generated in a numerical model of frontogenesis I: Model solutions, *Q. J. R. Meteorol. Soc.*, *122*, 1153–1174, 1996.
- Guest, F., M. Reeder, C. Marks, and D. Karoly, Inertia-gravity waves observed in the lower stratosphere over Macquarie Island, *J. Atmos. Sci.*, *57*, 737–752, 2000.
- Hamming, R. W., *Digital Filters*, Prentice-Hall, Old Tappan, N. J., 1983.
- Hertzog, A., C. Souprayen, and A. Hauchecorne, Observation and backward trajectory of an inertia-gravity wave in the lower stratosphere, *Ann. Geophys.*, *19*, 1141–1155, 2001.
- Hoskins, B. J., and F. P. Bretherton, Atmospheric frontogenesis models: Mathematical formulation and solution, *J. Atmos. Sci.*, *29*, 11–37, 1972.
- Hoskins, B. J., M. E. McIntyre, and A. W. Robertson, On the use and significance of isentropic potential vorticity maps, *Q. J. R. Meteorol. Soc.*, *111*, 877–946, 1985.
- Joly, A., et al., The Fronts and Atlantic Stormtracks Experiment (FASTEX): Scientific objectives and experimental design, *Bull. Am. Meteorol. Soc.*, *78*, 1917–1940, 1997.
- Joly, A., et al., Overview of the field phase of the Fronts and Atlantic Stormtracks Experiment (FASTEX) project, *Q. J. R. Meteorol. Soc.*, *125*, 1–33, 1999.
- Kalashnik, M. V., Forming of frontal zones during geostrophic adjustment in a continuously stratified fluid, *Izv. Russ. Acad. Sci. Atmos. Oceanic Phys.*, *Engl. Transl.*, *34*, 785–792, 1998.
- Kalashnik, M. V., Geostrophic adjustment and frontogenesis in a continuously stratified fluid, *Izv. Russ. Acad. Sci. Atmos. Oceanic Phys.*, *Engl. Transl.*, *36*, 386–395, 2000.
- Koch, S. E., and P. B. Dorian, A mesoscale gravity wave event observed during CCOPE. part III: Wave environment and possible source mechanisms, *Mon. Weather Rev.*, *116*, 2570–2591, 1988.
- Kunze, E., Near-inertial wave propagation in geostrophic shear, *J. Phys. Oceanogr.*, *15*, 544–565, 1985.
- Lalas, D. P., and F. Einaudi, On the characteristics of waves generated by shear layers, *J. Atmos. Sci.*, *33*, 1248–1259, 1976.
- Lane, T. P., M. J. Reeder, and T. L. Clark, Numerical modeling of gravity wave generation by deep tropical convection, *J. Atmos. Sci.*, *58*, 1249–1274, 2001.
- LeSommer, J., S. Medvedev, R. Plougonven, and V. Zeitlin, Singularity formation during relaxation of jets and fronts towards the state of geostrophic equilibrium, *Commun. Nonlinear Sci. Numer. Simul.*, *8*, 415–442, 2003.
- Ley, B. E., and W. R. Peltier, Wave generation and frontal collapse, *J. Atmos. Sci.*, *35*, 3–17, 1978.
- Lott, F., The transient emission of propagating gravity waves by a stably stratified shear layer, *Q. J. R. Meteorol. Soc.*, *123*, 1603–1619, 1997.
- Luo, Z., and D. C. Fritts, Gravity wave excitation by geostrophic adjustment of the jet stream. part II: Three dimensional forcing, *J. Atmos. Sci.*, *50*, 104–115, 1993.
- Moldovan, H., F. Lott, and H. Teitelbaum, Wave breaking and critical levels for propagating inertial gravity waves in the lower stratosphere, *Q. J. R. Meteorol. Soc.*, *128*, 713–732, 2002.
- O’Sullivan, D., and T. J. Dunkerton, Generation of inertia-gravity waves in a simulated life cycle of baroclinic instability, *J. Atmos. Sci.*, *52*, 3695–3716, 1995.
- Pavelin, E., J. A. Whiteway, and G. Vaughan, Observation of gravity wave generation and breaking in the lowermost stratosphere, *J. Geophys. Res.*, *106*, 5173–5179, 2001.
- Pfister, L., K. R. Chan, T. P. Bui, S. Bowen, M. Legg, B. Gary, K. Kelly, M. Proffitt, and W. Starr, Gravity waves generated by a tropical cyclone during the STEP tropical field program: A case study, *J. Geophys. Res.*, *98*, 8611–8638, 1993.
- Pierce, R. B., and T. D. A. Fairlie, Chaotic advection in the stratosphere: Implications for the dispersal of chemically perturbed air from the polar vortex, *J. Geophys. Res.*, *98*, 18,589–18,595, 1993.
- Plougonven, R., and H. Teitelbaum, Comparison of a large-scale inertia-gravity wave as seen in the ECMWF analyses and from radiosondes, *Geophys. Res. Lett.*, *30*(18), 1954, doi:10.1029/2003GL017716, 2003.
- Reeder, M. J., and M. Griffiths, Stratospheric inertia-gravity waves generated in a numerical model of frontogenesis. part II: Wave sources, generation mechanisms and momentum fluxes, *Q. J. R. Meteorol. Soc.*, *122*, 1175–1195, 1996.
- Reznik, G. M., V. Zeitlin, and M. Ben Jelloul, Nonlinear theory of geostrophic adjustment. part I. Rotating shallow-water model, *J. Fluid Mech.*, *445*, 93–120, 2001.
- Rosby, C. G., On the mutual adjustment of pressure and velocity distributions in certain simple current systems II, *J. Mar. Res.*, *1*, 239–263, 1938.
- Sato, K., A statistical study of the structure, saturation and sources of inertia-gravity waves in the lower stratosphere observed with the MU radar, *J. Atmos. Terr. Phys.*, *56*, 755–774, 1994.
- Scavuzzo, C. M., M. A. Lamfri, H. Teitelbaum, and F. Lott, A study of the low-frequency inertia-gravity waves observed during the Pyrénées experiment, *J. Geophys. Res.*, *103*, 1747–1758, 1998.
- Scinocca, J. F., and R. Ford, The nonlinear forcing of large-scale internal gravity waves by stratified shear instability, *J. Atmos. Sci.*, *57*, 653–672, 2000.
- Snyder, C., W. C. Skamarock, and R. Rotunno, Frontal dynamics near and following frontal collapse, *J. Atmos. Sci.*, *50*, 3194–3211, 1993.
- Sutherland, B. R., and W. R. Peltier, Internal gravity wave emission into the middle atmosphere from a model tropospheric jet, *J. Atmos. Sci.*, *52*, 3214–3235, 1995.
- Thomas, L., R. M. Worthington, and A. J. McDonald, Inertia-gravity waves in the troposphere and lower stratosphere associated with a jet stream exit region, *Ann. Geophys.*, *17*, 115–121, 1999.
- Uccellini, L. W., and S. E. Koch, The synoptic setting and possible energy sources for mesoscale wave disturbances, *Mon. Weather Rev.*, *115*, 721–729, 1987.
- Van Tuyl, A., and J. A. Young, Numerical simulation of nonlinear jet streak adjustment, *Mon. Weather Rev.*, *110*, 2038–2054, 1982.
- Zeitlin, V., S. B. Medvedev, and R. Plougonven, Frontal geostrophic adjustment, slow manifold and nonlinear wave phenomena in one-dimensional rotating shallow water. part 1: Theory, *J. Fluid Mech.*, *481*, 269–290, 2003.
- Zhang, F., S. E. Koch, C. A. Davis, and M. L. Kaplan, A survey of unbalanced flow diagnostics and their application, *Adv. Atmos. Sci.*, *17*, 165–183, 2000.
- Zhang, F., S. E. Koch, C. A. Davis, and M. L. Kaplan, Wavelet analysis and the governing dynamics of a large amplitude mesoscale gravity wave event along the east coast of the United States, *Q. J. R. Meteorol. Soc.*, *127*, 2209–2245, 2001.

R. Plougonven, Advanced Study Program, Mesoscale and Microscale Meteorology Division, National Center for Atmospheric Research, P.O. Box 3000, Boulder, CO 80307-3000, USA. (riwal.plougonven@polytechnique.org)

H. Teitelbaum and V. Zeitlin, Laboratoire de Météorologie Dynamique, Ecole Normale Supérieure, 24 rue Lhomond, F-75231 Paris Cedex 05, France. (teitel@lmd.ens.fr; zeitlin@lmd.ens.fr)